# Neonatal Fc receptor-targeted lignin-encapsulated porous silicon nanoparticles for enhanced cellular interactions and insulin permeation across the intestinal epithelium

João P. Martins [a],[**], Patrícia Figueiredo [a], Shiqi Wang [a], Erika Espo [a], Elena Celi [a],[b], Beatriz Martins [c], Marianna Kemell [d], Karina Moslova [d], Ermei Mäkilä [e], Jarno Salonen [e], Mauri A. Kostiainen [f], Christian Celia [b], Vincenzo Cerullo [c], Tapani Viitala [a], Bruno Sarmento [g],[h],[i], Jouni Hirvonen [a], Hélder A. Santos [a],[j],[*]

[a] Drug Research Program, Division of Pharmaceutical Chemistry and Technology, Faculty of Pharmacy, University of Helsinki, FI-00014, Helsinki, Finland
[b] Department of Pharmacy, University of Chieti – Pescara "G d'Annunzio", I-66100, Chieti, Italy
[c] Drug Research Program, Division of Pharmaceutical Biosciences, Faculty of Pharmacy, University of Helsinki, FI-00014, Helsinki, Finland
[d] Department of Chemistry, University of Helsinki, FI-00014, Helsinki, Finland
[e] Department of Physics and Astronomy, University of Turku, FI-20014, Turku, Finland
[f] Biohybrid Materials, Department of Bioproducts and Biosystems, Aalto University, FI-00076, Aalto, Finland
[g] i3S - Instituto de Investigação e Inovação em Saúde, University of Porto, 4200-135, Porto, Portugal
[h] INEB - Instituto de Engenharia Biomédica, University of Porto, 4200-135, Porto, Portugal
[i] CESPU - Instituto de Investigação e Formação Avançada em Ciências e Tecnologias da Saúde, 4585-116, Gandra, Portugal
[j] Helsinki Institute of Life Science (HiLIFE), University of Helsinki, FI-00014, Helsinki, Finland

## ARTICLE INFO

## ABSTRACT

Oral insulin delivery could change the life of millions of diabetic patients as an effective, safe, easy-to-use, and affordable alternative to insulin injections, known by an inherently thwarted patient compliance. Here, we designed a multistage nanoparticle (NP) system capable of circumventing the biological barriers that lead to poor drug absorption and bioavailability after oral administration. The nanosystem consists of an insulin-loaded porous silicon NP encapsulated into a pH-responsive lignin matrix, and surface-functionalized with the Fc fragment of immunoglobulin G, which acts as a targeting ligand for the neonatal Fc receptor (FcRn). The developed NPs presented small size (211 ± 1 nm) and narrow size distribution. The NPs remained intact in stomach and intestinal pH conditions, releasing the drug exclusively at pH 7.4, which mimics blood circulation. This formulation showed to be highly cytocompatible, and surface plasmon resonance studies demonstrated that FcRn-targeted NPs present higher capacity to interact and being internalized by the Caco-2 cells, which express FcRn, as demonstrated by Western blot. Ultimately, *in vitro* permeability studies showed that Fc-functionalized NPs induced an increase in the amount of insulin that permeated across a Caco-2/HT29-MTX co-culture model, showing apparent permeability coefficients ($P_{app}$) of $2.37 \times 10^{-6}$ cm/s, over the $1.66 \times 10^{-6}$ cm/s observed for their non-functionalized counterparts. Overall, these results demonstrate the potential of these NPs for oral delivery of anti-diabetic drugs.

## 1. Introduction

Type 1 diabetes mellitus (T1DM) is a chronic autoimmune disorder affecting millions of people all over the world, characterized by a partial or absolute loss of capability of the endocrine system to produce insulin [1]. Despite active research, T1DM remains non-reversible, non-curable,

and the number of patients is on the rise. The maintenance of normo-glycemic levels (the most effective manner of managing T1DM) is therefore dependent on the administration of exogenous insulin [1]. However, this requires, in most cases, the lifelong use of painful injections, multiple times per day, which deleteriously thwarts patient compliance [2,3]. In this scenario, an oral dosage form of insulin could significantly change the life of millions of diabetic patients who are still seeking for an effective, safe, easy-to-use, and affordable alternative to their insulin injections [2,4]. Oral insulin delivery would also reduce the high manufacturing costs associated with the sterile production requirements of injectable products [5], as well as the waste resulting from single-use disposable syringes and needles [6].

Nanotechnology-based drug carrier systems have already demonstrated to address multiple shortcomings of conventional therapies such as lack of specificity, burst release, cellular toxicity and severe side effects [7,8]. Thus, nanotechnology can benefit from advances in the fields of drug delivery and materials science to foster the development of a non-invasive, painless and patient compliant therapy for insulin administration [2]. However, the effectiveness of orally administered drugs, especially proteins like insulin, is hindered by several biological barriers, such as the low pH and enzymatic activity in the stomach, as well as the presence of mucus and an elaborate network of tight junctions in the intestinal epithelium [9]. Altogether, these physical and biochemical barriers impose a series of obstacles that result in poor drug absorption and, subsequently, poor bioavailability after oral administration [10].

The exploratory research around the development of nanosystems for oral drug delivery has already originated a myriad of nanoparticle (NP) platforms, produced according to a broad range of design aspects and fabrication techniques [11]. NPs generated over the years have shown to allow for the drugs to be released in a spatially and temporally controlled manner [12,13], to provide increased stability in the harsh conditions of the gastrointestinal tract (GIT) [12], to enhance the transmucosal drug delivery [14], to enable the specific targeting of cells or tissues [13,15,16], as well as to improve drug solubility and bioavailability after oral administration [16,17]. However, to the best of our knowledge, no nanoparticle-based insulin delivery system has reached the market yet, with invasive methods continuing to dominate the therapeutic landscape. Hence, the success of NP-based oral drug delivery demands a rational development of formulations that can simultaneously protect drugs from degradation in the GIT, while safely and efficiently shuttling them across the intestinal epithelium [5]. Such needs reinforce the continuous interest in the pursuit of new and improved NP systems, as well as the importance of a thorough exploration of organic and inorganic materials to this end. Moreover, the combination of organic–organic and organic–inorganic materials have shown to yield the fabrication of hybrid nanosystems that display a set of

advantages over non-hybrid ones, including higher encapsulation rates, specific release kinetics and higher stability [18], and which can be more suitable for the development of the multistage and stimuli-responsive NP systems that are required for successful oral drug delivery.

In this study, we designed a multistage NP system potentially capable of circumventing the highly dynamic microenvironmental changes of the GIT and the prohibitively low intestinal insulin absorption and bioavailability after oral administration (Scheme 1). This nanosystem consists of an insulin-loaded porous silicon NP encapsulated into a lignin matrix. The formed NPs were further surface-functionalized with a specific targeting ligand. Porous silicon NPs are versatile and heavily investigated drug carriers due to their highly tunable properties, high loading capacity, biocompatibility and biodegradability [19]. Lignin, the second most abundant natural organic polymer on earth, is usually a by-product of pulping and bio-refinery processes [20]. It is a renewable and eco-friendly material, which has only been explored very recently for drug delivery [21]. The fact that it is biocompatible, together with the possibility to chemically modify it to make it pH-sensitive, turn lignin into an especially suitable polymer for oral drug administration [22] and, in this particular case, for protecting the drug-loaded porous silicon NPs from the harsh conditions of the GIT. To the best of our knowledge, the potential of lignin for the oral administration of anti-diabetic drugs has not been explored yet. The Fc fragment of immunoglobulin G (IgG), chemically conjugated to the surface of the lignin matrices, served as targeting ligand for the neonatal Fc receptor (FcRn)-expressing intestinal cells. FcRn is a dual binding receptor, essential for immune surveillance and homeostatic regulation of IgG and albumin in the body [23]. The transcytosis and recycling of these abundant proteins across polarized epithelial barriers takes place inside of specialized vesicles, which protect them from catabolic degradation [24,25]. In humans, this receptor is expressed in the small intestine throughout adulthood at levels closely similar to the fetal expression, and diffusely expressed in the colon [26]. Recent studies showed hitherto undescribed possibilities for Fc-decorated NPs to enhance the transport of drug molecules across the intestinal epithelium and into the bloodstream following oral administration, via FcRn-mediated transcytosis [13,15,24,26].

Hence, we hypothesized that Fc-functionalized NPs could hijack the FcRn transcytotic pathway, being transported across the intestinal epithelium, and deliver insulin in the blood circulation, where it is expected to exert the therapeutic effect. For this purpose, we set out to explore the physicochemical properties of the developed nanosystem, including particle size and size distribution, surface charge and chemistry, morphology, pH-responsiveness, and *in vitro* insulin release profile. Also importantly, we investigated the cytocompatibility of the NPs, the interaction of both targeted and non-targeted NPs with FcRn-
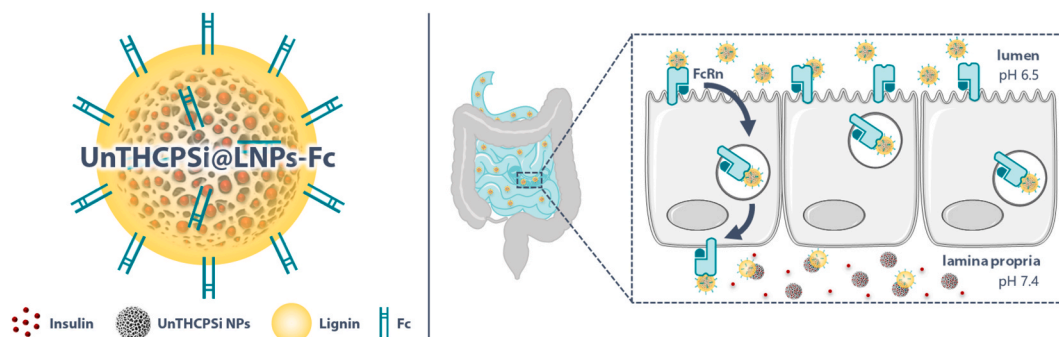


**Scheme 1. Schematic illustration of the multistage NP system designed in this study as a potential candidate for the administration of anti-diabetic drugs via the oral route.** The nanosystem consists of an insulin-loaded porous silicon NP encapsulated into a pH-responsive lignin matrix (LNPs). The surface of these pH-sensitive NPs was further surface-functionalized with the Fc fragment of IgG. When reaching the intestinal cells, Fc-functionalized NPs would hijack the FcRn-mediated transcytotic pathway, being transported across the cells, and releasing the drug in the basolateral compartment, allowing them to reach blood circulation. Image created using Servier Medical Art (Creative Commons - Attribution 3.0 Unported - CC BY 3.0).

expressing cells and, finally, the efficacy of FcRn-targeted NPs in increasing insulin permeation across the intestine, using an *in vitro* cell culture model, in which the FcRn expression was also studied.

## 2. Materials and methods

### 2.1. Materials

The materials and reagents used in this study are reported in detail in the Supporting Information.

### 2.2. Preparation of undecylenic acid modified thermally hydrocarbonized porous silicon (UnTHCPSi) NPs

UnTHCPSi NPs were prepared according to previously optimized protocols [17,27]. A detailed description of the preparation process can be found in the Supporting Information.

### 2.3. Chemical modification of lignin

Two variants of lignin were prepared by chemical modification: carboxylated lignin and maleimide-terminated lignin. These modifications were performed in BioPiva™ softwood kraft lignin (molecular weight 5 kDa). To increase the amount of carboxyl groups on its structure, lignin was carboxylated as described elsewhere [22]. Briefly, 200 mg of BioPiva™ softwood kraft lignin was incubated with 400 mg of succinic anhydride (22.2 mmol) and 40 mg of 4-dimethylaminopyridine (DMAP; 4.1 mmol) in 30 mL of tetrahydrofuran (THF), and stirred for 48 h at room temperature (RT). To remove the unreacted reagents, the reaction mixture was transferred to a dialysis bag (Spectra/Por® 1 Standard RC Dry Dialysis Tubing, 12–14 kDa, Spectrum Labs, CA, USA), and dialyzed against Milli-Q water, which was replaced periodically during 48 h. The carboxylated lignin was freeze-dried and stored for further use.

To modify the lignin with maleimide groups, which will be later used for chemical conjugation, 200 mg of BioPiva™ softwood kraft lignin was mixed with 10 mL of THF. In parallel, 37.4 mg of *N*,*N*′-Dicyclohexylcarbodiimide (DCC) was dissolved in 3.3 mL of THF, 88.6 mg of *N*-Mal-*N*-bis(PEG2-acid) was dissolved in 3.3 mL of THF, and 2 mg of DMAP was dissolved in 3.3 mL of THF. Each of the three solutions were added to the initial lignin solution, in this order, and stirred for 24 h at RT. The reaction mixture was transferred to a dialysis bag, and dialyzed against Milli-Q water, following the protocol described above. The maleimide-terminated lignin was freeze-dried and stored for further use.

Fourier transform infrared spectroscopy (FTIR; VERTEX 70, Bruker, MA, USA) using a horizontal attenuated total reflectance (ATR) accessory (MIRacle, PIKE Technologies, WI, USA) was used to characterize the chemical modifications of lignin. The ATR-FTIR spectra were recorded between 4000 and 650 cm$^{-1}$, with a resolution of 4 cm$^{-1}$, using OPUS 5.5 software. Additionally, maleimide-terminated lignin was characterized by $^1$H nuclear magnetic resonance (NMR) spectroscopy, after being dissolved in deuterated dimethyl sulfoxide (DMSO-d$_6$), at RT. The spectra were recorded on a an Avance III 400 MHz NMR spectrometer (Bruker, Swizerland) and analyzed by MestReNova software.

### 2.4. Insulin loading into UnTHCPSi NPs

Human recombinant insulin was loaded into the UnTHCPSi NPs by an immersion method, as described elsewhere [14,19]. Briefly, 1 mg of UnTHCPSi NPs was dispersed in 500 μL of Milli-Q water by tip sonication, and immersed in an insulin solution (2.25 mL, 200 μg/mL in 0.01 M HCl). The mixture was stirred at RT for 90 min (300 rpm). Then, the NPs were collected by centrifugation at 16,110×*g* (5415D, Eppendorf, Germany) for 5 min, to remove the excess unloaded insulin, and washed once with 1 mL of Milli-Q water.

### 2.5. Nanoencapsulation of insulin-loaded UnTHCPSi NPs into lignin

The insulin-loaded UnTHCPSi NPs were encapsulated into lignin by desolvation, yielding the formation of UnTHCPSi@LNPs. Briefly, carboxylated lignin and maleimide-terminated lignin (ratio 70:30) were dissolved in 70% (v/v) EtOH to a concentration of 1 mg/mL for 1 h, under magnetic stirring. The solution was then filtered using an Acrodisc® 13 mm Syringe Filter, 0.45 μm pore size. 250 μg of insulin-loaded UnTHCPSi NPs were dispersed in 570 μL of Milli-Q water by tip-sonication, and then mixed with 430 μL of lignin solution. The mixture was stirred overnight at RT, without sealing the incubation flask. The LNPs were formed by nanoprecipitation and collected by centrifugation at 16,110×*g* (5415D, Eppendorf, Germany) for 5 min after complete evaporation of the organic solvent. Then, the excess, non-precipitated lignin was removed by washing the NPs twice with Milli-Q water.

### 2.6. Conjugation of Fc to insulin-loaded UnTHCPSi@LNPs

The Fc fragment of IgG was covalently conjugated to the surface of insulin-loaded UnTHCPSi@LNPs by maleimide-thiol chemistry. 2-Iminothiolane (Traut's reagent; 5.5 μL from a 5 mg/mL solution in 5 mM ethylenediaminetetraacetic acid (EDTA) in phosphate-buffered saline (PBS)) was mixed with 43 μL of Fc fragment (2.3 mg/mL) to modify the NH$_2$ groups of the Fc fragment with thiol groups (Fc-SH). The mixture was stirred for 1 h at 37 °C. Afterwards, 1 mg of NPs were dispersed in PBS (pH 6.5; 3 mg/mL), and the thiolated Fc fragments were added to the NP suspension and allowed to react at 4 °C for 1 h, under magnetic stirring, forming insulin-loaded UnTHCPSi@LNPs-Fc. Then, the NPs were collected by centrifugation at 16,110×*g* (5415D, Eppendorf, Germany) for 5 min, and washed once with Milli-Q water to remove the unconjugated Fc.

### 2.7. Physicochemical characterization of the NPs

The physicochemical properties of the developed NPs were characterized by a variety of techniques, including dynamic light scattering (DLS) and electrophoretic laser scattering (ELS), ATR-FTIR, elemental analysis, transmission electron microscopy (TEM) and exergy dispersive X-ray (EDX).

#### 2.7.1. Size and surface charge

The average particle size (*z*-average), polydispersity index (PdI) and zeta (ζ)-potential were characterized by DLS-ELS, upon analyzing NPs dispersed in Milli-Q water using a Malvern Zetasizer Nano ZS instrument (Malvern Ltd., UK).

#### 2.7.2. Surface chemical modifications

A Bruker VERTEX 70 FTIR (Bruker, MA, USA) spectrometer coupled with a horizontal ATR sampling accessory (MIRacle, PIKE Technologies, WI, USA) was used to evaluate the chemical modifications taking place on the surface of the UnTHCPSi NPs (encapsulation into LNPs and conjugation with Fc fragment). A minimum of 200 μg of NPs were collected by centrifugation and left to dry overnight. The measurements were performed at RT with a resolution of 4 cm$^{-1}$.

The amount of Fc chemically conjugated to the surface of the UnTHCPSi@LNPs-Fc was evaluated by elemental analysis, based on the chemical structure of the targeting ligand. For that purpose, the number of atoms of carbon (C), nitrogen (N) and sulfur (S) in the amino acid sequence of the Fc molecule were counted. The final molecular weight of the Fc fragment obtained herein supported the correct counting of the atoms [28]. A Vario Micro cube CHNS analyzer (Elementar Analysensysteme, GmbH, Germany) recorded the percentages of C, N and S present in dry NP samples, with and without Fc. The percentages of these elements in non-conjugated UnTHCPSi@LNPs was subtracted to the percentages measured in Fc-conjugated NPs and converted to mass

of element per gram of UnTHCPSi@LNPs. The mass of each element was divided by its atomic number, to obtain the number of mols, which was further multiplied by the number of atoms of that same element in the Fc molecule. When multiplying the molarity of Fc per gram of UnTHCPSi@LNPs by the molecular weight of the Fc fragment, it was possible to obtain the abundance of Fc per gram of UnTHCPSi@LNPs.

### 2.7.3. Morphology and presence of Si in the NPs

The morphology of the developed NPs at different steps of preparation was assessed by TEM, a commonly used microscopic technique that uses electron beams to characterize the shape of nanomaterials [29]. Briefly, 10 μL of an aqueous NP suspension was placed on top of carbon-coated copper grids for 3–5 min. Then, the droplet was blotted away, and the grids were left to dry overnight at RT, before imaging with a Tecnai™ F12 microscope (FEI Company, USA). Additionally, an Oxford INCA 350 EDX spectrometer (Oxford Instruments, UK) connected with a field emission scanning electron microscope (FESEM; Hitachi S-4800, Japan) was used to verify the presence of Si in the NPs [30]. The measurements were performed in areas imaged with the bright field TE detector of the FESEM.

### 2.8. pH-Responsiveness of the developed LNPs

Lignins are known to resist the harsh conditions of the GIT, as the incomplete ionization of the carboxylic groups hinders their solubility at acidic pH [31], which makes them capable of protecting insulin from premature release and degradation in the stomach. For this reason, the dissolution behavior of the LNPs was evaluated at different pH conditions. Briefly, 250 μg of UnTHCPSi@LNPs, UnTHCPSi@LNPs-Fc and insulin-loaded UnTHCPSi@LNPs-Fc were separately dispersed in 1 mL of buffer solutions at different pH values: 0.1 M hydrochloric acid (HCl; pH 1.2), 2-(N-morpholino)-ethanesulfonic acid (MES; pH 5.5, pH 6.0 and pH 6.5), and phosphate-buffered saline (PBS; pH 7.4), to mimic the pH conditions found by the orally administered NPs throughout the GIT and in the blood circulation. The mixtures were kept at 37 °C under magnetic stirring. Samples were collected 2 min, 15 min and 30 min after starting the incubation, and analyzed by DLS-ELS and TEM, as described above.

### 2.9. Association efficiency (AE), loading degree (LD) and insulin release profile

#### 2.9.1. AE and LD

The AE and LD were calculated to determine the amount of insulin loaded into the developed NPs and that can be released to exert a therapeutic effect. To promote the release of insulin, the NPs were dispersed into PBS – fetal bovine serum (FBS; 10%; pH 7.4) and stirred overnight (300 rpm; IKA® RT 15, Germany) at 37 °C. For the drug loading, the NPs were accurately weighed after centrifugation and drying. The percentages of AE and LD were determined by the direct method, using Eq. (1) and (2):

$$AE~(\%) = \frac{Insulin~released~from~UnTHCPSi@LNPs-Fc}{Initial~amount~of~insulin} \times 100 \quad (1)$$

$$LD~(\%) = \frac{Insulin~released~from~UnTHCPSi@LNPs-Fc}{Total~mass~of~the~NPs~(\mu g)} \times 100 \quad (2)$$

The concentration of insulin in the samples was determined by high-performance liquid chromatography (HPLC; Agilent 1260, Agilent Technologies, USA), as previously described [15]. Briefly, a $C_{18}$ column (4.6 × 150 mm, 5 μm, Supelco Discovery®, USA) was used as stationary phase, whereas 0.1% trifluoroacetic acid (TFA; pH 2.0) and acetonitrile (ACN) were used as the mobile phase, under a gradient system. The initial ratio of 0.1% TFA to ACN was 80:20 (v/v) was changed to 70:30 (v/v) during 7 min, and then again changed to 80:20 (v/v) for the last 3 min, always under a flow rate of 1.2 mL/min. The injection volume was

50 μL and the detection wavelength was 240 nm. The temperature of the column was set to RT. The total area under the curve (AUC) was used to quantify the concentration of insulin in the samples. The data reported corresponds to the averages of three technical replicates.

#### 2.9.2. Insulin release profile

The insulin release profile was performed in buffer solutions at different pH conditions, to mimic the passage of the NPs through the GIT and blood circulation. To investigate the release of the drug in the stomach conditions, UnTHCPSi@LNPs-Fc equivalent to 30 μg of insulin were firstly dispersed in 10 mL of HCl 0.1 M (pH 1.2), and stirred for 2 h. Afterwards, the NPs were collected by centrifugation and re-dispersed in 10 mL of PBS (pH 6.5). The mixture was stirred for the next 6 h, to investigate the release of the drug in the pH conditions mimicking the intestine, and in which the FcRn-mediated transcytosis must occur [25]. The NPs were again collected by centrifugation, and dispersed in PBS – FBS (10%; pH 7.4), to investigate the release in pH conditions mimicking the blood circulation. The mixture was stirred for 3 h. Insulin-loaded UnTHCPSi NPs and UnTHCPSi@LNPs were used as control, and their initial concentrations adjusted to an equivalent amount of 30 μg of insulin. The entire experiment was conducted under magnetic stirring (300 rpm; IKA® RT 15, Germany) at 37 °C, in triplicates. At different time points, from 15 min to 11 h, 500 μL samples were withdrawn for analysis, and the same volume of pre-warmed buffer solutions (HCl, PBS or PBS – FBS (10%), respectively) was replaced, to maintain the release volumes. The collected samples were centrifuged at 16,110×g (5415D, Eppendorf, Germany) for 5 min, and the supernatants were analyzed using HPLC, as described above.

### 2.10. Cell culturing

Human epithelial colorectal adenocarcinoma Caco-2 and hepatocellular carcinoma HepG2 were obtained from American Type Culture Collection (ATCC®, USA). Human goblet-like HT29-MTX cells were kindly provided by Dr. T. Lesuffleur (INSERM U178, Villejuif, France). Caco-2 (passage #26 – 40), HepG2 (passage #18 – 32) and HT29-MTX (passage #32 – 40) were grown separately in cell culture flasks. Complete medium consisting of Dulbecco's Modified Eagle Medium (DMEM) supplemented with 10% (v/v) FBS, 1% (v/v) L-glutamine, 1% (v/v) non-essential amino acids (NEEA) and 1% (v/v) antibiotic – antimitotic mixture (100 U/mL penicillin and 100 U/mL streptomycin; Pen-Strep). The medium used for HepG2 cell culturing was further supplemented with 1% (v/v) sodium pyruvate. All cell lines were kept at 37 °C, 5% $CO_2$ and 95% relative humidity, in a 16 BB gas incubator (Heraeus Instruments, GmbH, Germany). Cell culture medium was changed every two days. Sub-culturing was performed when cells reached 80% confluency. The medium was discarded, and the flasks were washed twice with PBS – EDTA. To detach them from the flasks, cells were incubated with 0.25% (v/v) trypsin in PBS – EDTA for 4 min. After centrifugation, cells were dispersed in fresh, pre-warmed cell culture medium, and transferred to new culture flasks.

### 2.11. Western blot analysis of the FcRn expression

The expression of the FcRn in intestinal cells was evaluated by Western blot. Caco-2, HT29-MTX and Caco-2/HT29-MTX (ratio 90:10) cell suspensions were grown in 6-well plates or 6-well Transwell® permeable supports for 7, 14 and 21 days, according to the purpose of the study. HepG2 cells were used as positive control. Cells were scrapped and the protein was extracted. The protein concentrations of each lysate were determined using a Bradford Assay. Extracts were resolved by SDS-PAGE using a 4–20% gel under reducing conditions, and proteins were transferred onto a polyvinylidene difluoride (PVDF) membrane. The membrane was blocked using 2% (w/v) non-fat milk, and blots were probed with Human FCRN Antibody (MAB8639) overnight at 4 °C. Afterwards, bound antibody was detected with Alexa Fluor® 488

conjugate anti-mouse IgG (H + L), F (ab')$_2$ Fragment. Blocking, incubations and washings were performed using Tris Buffered Saline (TBS) with 0.1% (v/v) Tween® 20. Signal was detected by chemiluminescence (ChemiDoc™ MP Imaging System, BioRadiations Life Science Research, CA, USA). Reactions were normalized to a monoclonal mouse *anti*-α-tubulin.

### 2.12. Cytocompatibility studies

The cytocompatibility of the herein developed NPs with intestinal cells was assessed using CellTiter-Glo® Luminescent Cell Viability Assay, as previously reported [13]. Briefly, 100 μL of Caco-2, HT29-MTX and Caco-2/HT29-MTX (ratio 90:10) were seeded in 96-well microplates at a density of $5 \times 10^4$ cells/mL. Cells were kept at 37 °C, 5% CO$_2$ and 95% relative humidity and allowed to attach for 24 h. Then, the culture medium was discarded, and 100 μL of NP suspensions (UnTHCPSi, UnTHCPSi@LNPs and UnTHCPSi@LNPs-Fc) in cell culture media were added to the cells, at concentrations of 25, 50, 100, 200 and 400 μg/mL, and incubated for 6 and 24 h at 37 °C, in a humidified atmosphere. 1% (v/v) Triton X-100 and cell culture media were used as positive and negative control, respectively, and incubated with the cells in the same manner. Afterwards, cells were brought to RT and washed twice with pre-warmed Hank's balanced salt solution − 4-(2-hydroxyethyl)-1-pipezarinethanesulfonic acid (HBSS − HEPES). 100 μL of CellTiter-Glo® assay reagent previously diluted in HBSS − HEPES (ratio 1:1) were added to the cells, and incubated at RT for 10 min. The plate was shaken for 2 min to ensure mixing and measured using a Varioskan Lux Multimode Microplate Reader (Thermo Fisher Scientific, Waltham, MA, USA). The quantification of the metabolically active cells was based on the amount of adenosine triphosphate content (ATP) produced by the viable cells. Data corresponds to the averages of four independent measurements ($n = 4$).

### 2.13. Fc fragment binding ability and cell–NP interaction studies

The binding ability of the Fc fragments and Fc-functionalized NPs was studied by surface plasmon resonance (SPR). SPR measurements were performed with a Navi™ 200 OTSO (BioNavis Ltd, Finland) equipped with four flow channels, and a Navi™ 210 A VASA (BioNavis Ltd, Finland) equipped with two flow channels. Both instruments were equipped with two laser wavelengths (670 nm and 780 nm), in which the linearly p-polarized laser lights were directed through an equilateral prism coupled to a glass side (∼2 mm) coated with a gold layer (∼50 nm), using the Kretschmann configuration. Prior to the experiments, the gold-coated SPR sensors (BioNavis Ltd, Finland) were cleaned by immersion in a solution of 30% (v/v) hydrogen peroxide, 30% (v/v) ammonia hydroxide, and Milli-Q water (1:1:5 v/v) and boiled for 5 min. After that, the sensors were thoroughly rinsed with water and dried with N$_2$ before use. The flow channel injections were done using a Ismatec™ Reglo Digital MS-2/12 multichannel pump (Cole-Parmer, Germany).

#### 2.13.1. Binding affinity of the free Fc fragments

Firstly, SPR measurements were used to investigate the binding affinity of the free Fc fragments, and this was performed using *Staphylococcal* protein A (SPA or protein A), a protein composed of five homologous domains capable of binding the Fc portion of IgGs [32]. The gold-coated sensors were cleaned in oxygen plasma for 10 min at ∼1000–1200 mTorr. Afterwards, the sensors were rapidly transferred into a 200 μM solution of dithiobis (succinimidyl propionate) (DSP) dissolved in DMSO and incubated for 2 h at RT for thiol linkage. The DSP coated sensors were rinsed with DMSO, then with PBS, and incubated overnight at 4 °C with a 0.5 mg/ml protein A solution in PBS. After that, the sensors were transferred into a 1 M ethanolamine solution (pH 8.6) for 30 min–1 h, to block residual reacting sites. Finally, the sensors were washed with Milli-Q water, dried with air or N$_2$, and stored at 4 °C. This experiment was conducted on the Navi™ 200 OTSO. The full SPR

reflectance spectrum was measured between 58 and 75°, and scanned with a 670 nm laser wavelength, with a scanning time of ∼2 s. Flow channels and fluidic paths were firstly injected with PBS and then primed with the assay buffer (HBSS–HEPES, pH 7.4) for initial signal stabilization. Once achieving a stable baseline, the Fc fragment solutions (0.1–100 μg/mL in HBSS–HEPES, pH 7.4) were injected at a flow rate of 30 μL/min, until reaching the equilibrium (association rate equal to the dissociation rate). At this point, HBSS–HEPES was injected for 50 min, to remove unbound excess Fc fragments.

#### 2.13.2. pH-dependent binding of Fc fragments to protein A

The influence of the pH on the binding ability of the Fc fragments to protein A was investigated. This experiment conducted on a Navi™ 200 OTSO and protein A was immobilized on the surface of the gold-coated SPR sensor as described above. The incident light wavelength used was 670 nm, and the full SPR reflectance spectrum was measured between 55 and 77° every 3 s. Flow channels and fluidic paths were primed with HBSS–HEPES at pH 6.5, 7.4 and 8.2.1 mg/mL BSA was injected in the system for 5 min to block residual reacting sites. HBSS–HEPES at the corresponding pH values was again injected until a stable baseline was achieved. 10 μg/mL Fc fragment solutions in HBSS–HEPES (pH 6.5, 7.4 and 8.2) were injected for 40 min at a flow rate of 30 μL/min.

#### 2.13.3. Binding of FcRn-targeted NPs to Caco-2 cells

The cell−NP interactions were investigated by assessing the binding ability of FcRn-targeted and non-targeted NPs to Caco-2 cells. For this, Caco-2 cells were seeded over a gold-coated SPR sensor at a concentration of $8.8 \times 10^5$ cells/mL, and allowed to attach for 24 h at 37 °C, 5% CO$_2$ and 95% relative humidity. Afterwards, the sensor was transferred onto a clean 35 mm Petri dish with 2 mL of cell culture medium, and maintained in a humidified atmosphere for 14 days, with growing medium replaced every other day. This experiment was performed on a Navi™ 210 A VASA, with an incident laser wavelength of 670 nm, and the full SPR reflectance spectrum was measured between 55 and 77° every 3 s. The temperature of the system was set at 37 °C. HBSS–HEPES–PS (pH 6.5) was injected into the system for initial signal stabilization. Then, 100 μg/mL suspensions of UnTHCPSi@LNPs and UnTHCPSi@LNPs-Fc in HBSS–HEPES–Pen-Strep (pH 6.5) were injected at a flow rate of 25 μL/min for 30 min, followed by a 30 min injection of buffer. Data collected from all SPR experiments were exported in ASCII format with MP-SPR Navi Data Viewer 4.2.5 software by using the centroid method for determining the SPR peak angular position (PAP).

### 2.14. In vitro permeability studies

Permeability studies were performed in Caco-2/HT29-MTX (ratio 90:10) cell monolayers seeded at a density of $6.8 \times 10^4$ cells/cm$^2$ in 6-well Transwell® permeable supports (0.4 μm pore size; Corning Inc., NY, USA) and grown for 21 days. Culture media was replaced every other day. The successful formation of tight junctions, and therefore, of a barrier-like structure was evaluated by monitoring the transepithelial electrical resistance (TEER) throughout the culture period, using a Millicell ERS-2 volt-ohm-meter with STX01 electrodes (Millipore, MA, USA). A detailed description of the TEER measurements is reported in the Supporting Information.

At the end of the culture period, the TEER was again monitored, the monolayers were washed with HBSS–HEPES, and maintained for 15 min in this buffer for equilibration. Insulin permeability was investigated from the apical (0.5 mL) to the basolateral (1.5 mL) compartment, using HBSS–HEPES pH 6.5 and pH 7.4, respectively. Insulin-loaded NPs (UnTHCPSi, UnTHCPSi@LNPs and UnTHCPSi@LNPs-Fc) equivalent to 8 μg of insulin were added to the apical compartments of the Transwell® membranes. The plates were kept at 37 °C, with shaking (100 rpm). At specific time points (15–120 min), 300 μL samples were collected from the basolateral compartments, and the same volume of pre-warmed HBSS–HEPES (pH 7.4) was added to maintain a constant volume. The

concentration of insulin in the basolateral compartments was quantified by HPLC, as described above, and the apparent permeability coefficients ($P_{app}$) were calculated using Eq. (3)

$$P_{app} = \frac{\Delta Q}{\Delta t} \times \frac{1}{AC_0} \qquad (3)$$

where, $\Delta Q/\Delta t$ is the steady-state flux (µg/s), $C_0$ is the initial insulin concentration in the apical compartment (µg/mL), and $A$ is the surface area of the filter (cm$^2$). The $P_{app}$ values were estimated using $C_0$ values based on the complete insulin release from the NPs.

At the end of the study, the monolayers were washed with HBSS–HEPES, to remove the excess NPs that were not interacting with the cells, and fixed with glutaraldehyde at RT for 15 min. After washing again, the membranes were dehydrated and embedded in epoxy resin for TEM analysis. Ultra-thin sections of the membranes cut in the perpendicular direction were stained with uranyl acetate and lead citrate and observed under the microscope. The experiments were carried out in triplicate ($n = 3$).

### 2.15. Statistical analysis

The experiments conducted in this study were performed, at least, in triplicates ($n \geq 3$), and the results are reported as mean ± standard deviation (*s.d.*). The statistical significances were analyzed by one-way or two-way analysis of variance (ANOVA), followed by the Bonferroni *post hoc* test (GraphPadPrism, GraphPad Software Inc., CA, USA). The levels of significance were set at probabilities of *$p < 0.05$, **$p < 0.01$, ***$p < 0.001$, and ****$p < 0.0001$.

## 3. Results and discussion

### 3.1. Characterization of the carboxylated lignin and maleimide-terminated lignin

Lignin is a renewable resource and one of the most abundant polymers derived from biomass on Earth [22,33,34]. Its eco-friendly origin, biocompatibility, biodegradability and low toxicity have turned it into an exciting material for the development of advanced drug delivery

systems [21,35]. In this study, softwood kraft lignin was chemically modified to render it with a pH-responsive dissolution behavior and, simultaneously, a suitable surface chemistry for the development of a targeted drug delivery system for oral administration.

The chemical structure of the native lignin used in this study has been previously reported [36]. The amount of carboxylic groups in its structure was increased by reacting the native hydroxyl groups with succinic anhydride, using DMAP as a nucleophilic catalyst [37]. The scheme of lignin carboxylation is shown in Fig. 1a. Here, a nucleophilic attack of catalyst DMAP on a carbonyl group of succinic anhydride forms a tetrahedral intermediate, which triggers a more activated nucleophilic attack to the hydroxyl groups present on lignin than that of the original anhydride [36]. The reaction of this intermediate with the hydroxyl groups of lignin leads to the formation of a second intermediate, which collapses, followed by the elimination of the pyridine group, and the lignin carboxylation reaction is completed [36]. In turn, the inclusion of maleimide groups in the structure of lignin, which will be further used for conjugation reactions, was achieved by reacting lignin with a heterofunctional PEG linker (Fig. 1b). In this reaction, DCC was used as a coupling agent and DMAP as a catalyst [38].

The success of the chemical modifications was evaluated by ATR−FTIR and $^1$H NMR. The ATR−FTIR spectrum showed that native lignin displays the typical bands that correspond to the presence of different functional groups on its structure [39]. The spectrum of the carboxylated lignin, in turn, showed a stronger absorbance band at 1720 cm$^{-1}$, as highlighted in purple in Fig. 1c, which is attributed to the stretching vibrations of C=O of the free –COOH groups and of C=O from a ketone group at β-location [36,39].

In the case of the maleimide-terminated lignin, the increase in the IR absorption band at *ca.* 1710 cm$^{-1}$ is attributed to the C=O stretching present in maleimide. This is supported by the spectra of the linker alone and the physical mixture between the linker and native lignin when compared to the spectrum of native lignin (Fig. 1c, highlighted in blue). The ATR−FTIR data of the maleimide-terminated lignin was further supported by the $^1$H NMR. In this case, the spectra of the linker alone showed a chemical shift at 7 ppm, which derives from the protons in the maleimide molecule (Fig. 1d). The same peak appears in the chemically modified lignin, but not in the native lignin, supporting the success of
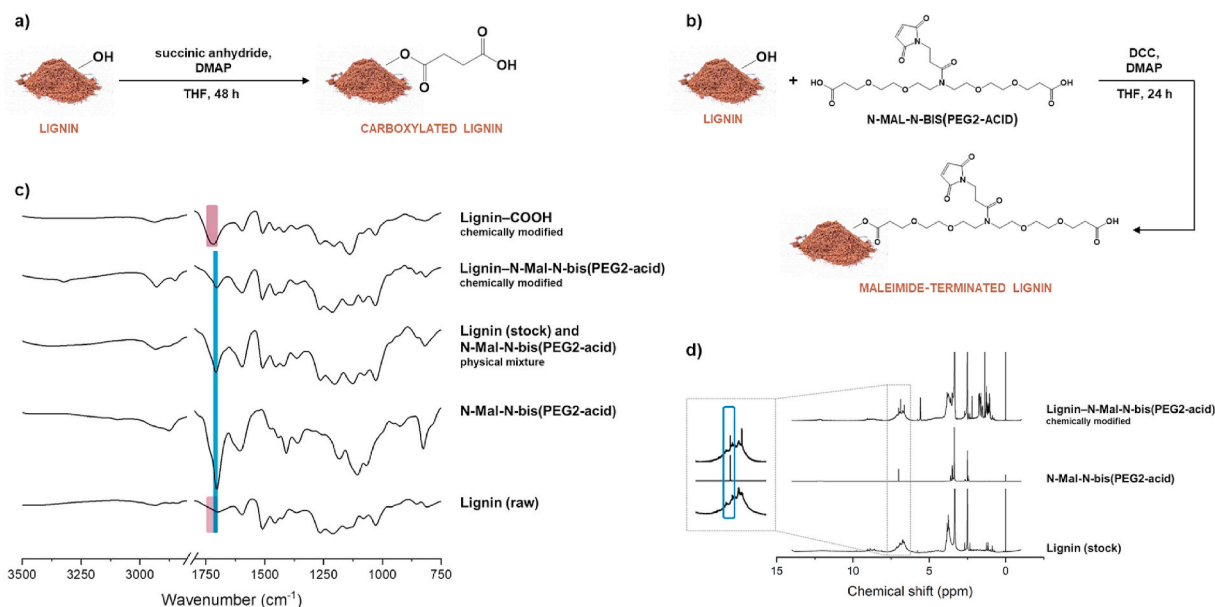


**Fig. 1. Lignin chemical modification.** Schematic representation of **a)** lignin carboxylation reaction and **b)** lignin chemical modification with a maleimide-terminated heterofunctional PEG linker (*N*-Mal-*N*-bis [PEG2-acid]); **c)** ATR−FTIR spectra, from bottom to top, of BioPiva™ softwood kraft lignin (raw), *N*-Mal-*N*-bis(PEG2-acid), their physical mixture, lignin that was chemically modified with the maleimide-terminated *N*-Mal-*N*-bis(PEG2-acid), and carboxylated lignin; **d)** $^1$H NMR spectra of lignin (stock), *N*-Mal-*N*-bis(PEG2-acid), and lignin after chemical modification with *N*-Mal-*N*-bis(PEG2-acid).

the reaction.

### 3.2. Physicochemical characterization of the NPs

The NP system developed in this study consists of an insulin-loaded UnTHCPSi NP encapsulated into a lignin matrix, and further surface-functionalized with the Fc fragment of IgG. UnTHCPSi NPs were used

as drug carriers due to their high loading capacity, biodegradability, biocompatibility, as well as capability to be loaded with a variety of therapeutic compounds, such as proteins and peptides [40,41]. These NPs were prepared using a top-down approach by the electrochemical anodization of $p^+$-type monocrystalline Si wafers into porous films, followed by surface stabilization by thermal hydrocarbonization, surface modification using undecylenic acid treatment, and then milling,
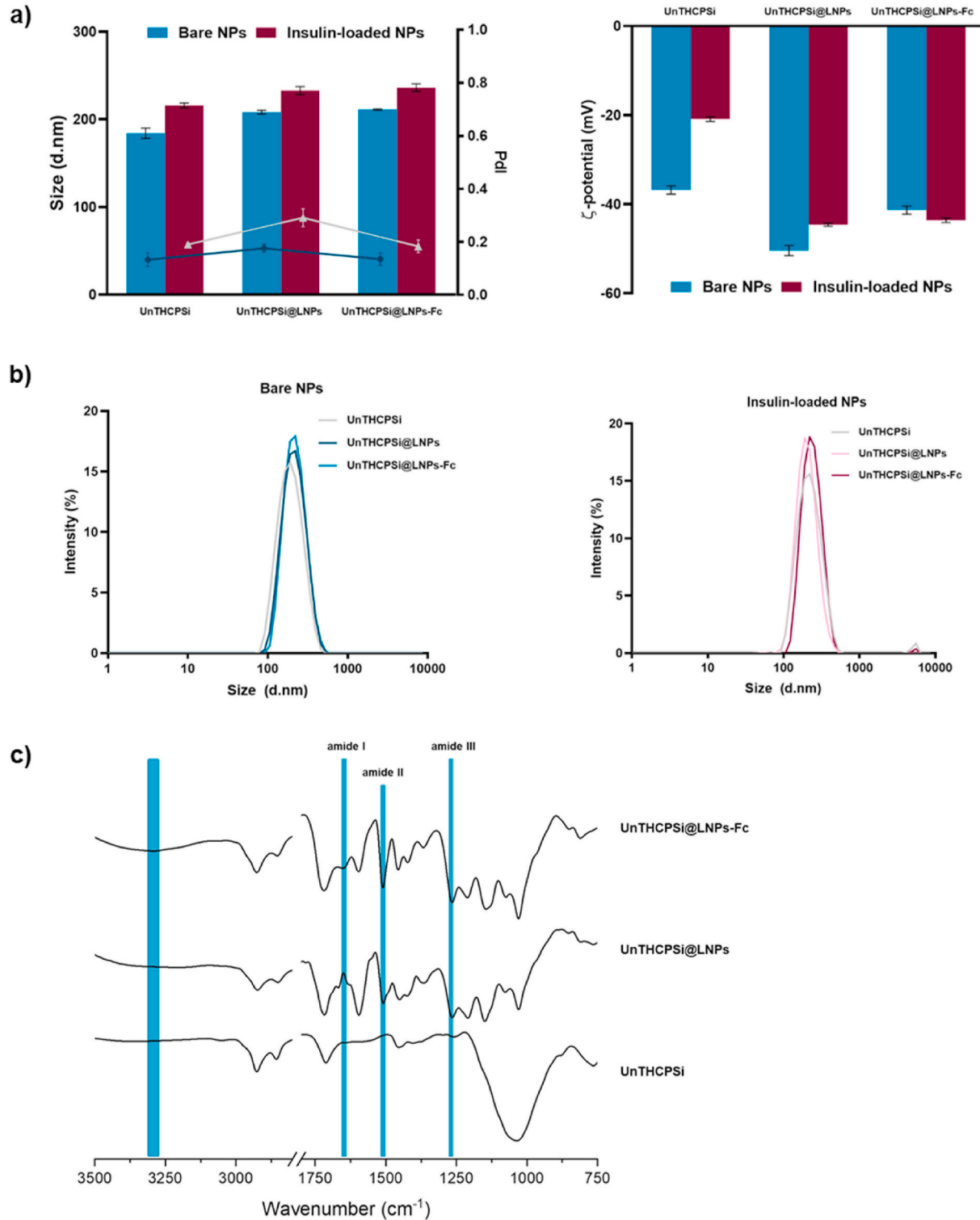


**Fig. 2. Physicochemical characterization of the NPs developed in this study. a)** Size, PdI, ζ-potential and **b)** size distribution by intensity of bare and insulin-loaded UnTHCPSi NPs, UnTHCPSi@LNPs and UnTHCPSi@LNPs-Fc. Results are expressed as mean $\pm$ s.d. of three independent measurements of the same batch ($n = 3$). **c)** ATR−FTIR spectra of the NPs at different steps of preparation.

according to previously optimized protocols [17,27]. The detailed characterization of the physical properties of the UnTHCPSi NPs by $N_2$ sorption at $-196\ ^\circ C$ are shown in Table S1. Here, insulin was used as a model anti-diabetic drug and it was loaded into the UnTHCPSi NPs by an immersion method [14,19].

Insulin-loaded UnTHCPSi NPs were further encapsulated into a lignin matrix, using a ratio of carboxylated:maleimide-terminated lignin of 70:30 (w/w), based on the optimization of the encapsulation protocol (data not shown). The NPs, previously dispersed in water, were mixed with a lignin solution in EtOH, and maintained under mechanical agitation. The subsequent solvent-evaporation process led to the formation of individual lignin matrices around the core NPs *via* nano-precipitation, which is an easy, reliable and high-yield procedure that does not require the use lots of instrumentation or chemicals. The Fc fragment of IgG, previously modified with thiol groups (Fc-SH), was further conjugated to the surface of the NPs via maleimide-thiol chemistry [26].

The DLS data showed sizes of $184 \pm 6$ nm for the UnTHCPSi NPs, which increased up to $208 \pm 2$ nm after encapsulation into the lignin matrices (Fig. 2a). The functionalization of the UnTHCPSi@LNPs with the Fc fragment did not significantly affect the size of the NPs ($211 \pm 1$ nm), as expected, since the Fc is a very small molecule (Fig. 2a). Overall, the NPs presented a narrow size distribution throughout the preparation steps, with the final formulation presenting values of $0.14 \pm 0.02$ when bare, and $0.18 \pm 0.02$ when loaded with insulin (Fig. 2a and b). The insulin-loaded NPs showed a consistent but mild increase in the NP size and PdI throughout the preparation process, which had a minimal effect on the size of the NPs, as later proved by the TEM imaging. The size of the final formulation is suitable for cellular uptake at the intestinal level [42,43], which is essential to ensure that the NPs can be internalized by the epithelial cells. The $\zeta$-potential of the UnTHCPSi NPs was highly negative ($-37 \pm 1$ mV), as previously reported [13,15], becoming even more negative after encapsulation with lignin ($-50 \pm 1$ mV) [36], then showing a slight increase once functionalized with the Fc fragment ($-41 \pm 1$ mV), an effect that has also been observed in previous works (Fig. 2a) [13]. Interestingly, the surface charge of insulin-loaded UnTHCPSi NPs was higher than their non-loaded counterparts ($-21 \pm 1$ mV), which supports the possible deposition of insulin on the surface (Fig. 2a). Yet, the variations in the $\zeta$-potential observed in the insulin-loaded NPs throughout the preparation steps were coherent with those observed in the unloaded ones.

ATR–FTIR spectroscopy of the NPs throughout the preparation steps showed the characteristic bands of the UnTHCPSi NPs (Fig. 2c) [13,15], becoming visibly changed with the presence of lignin in the formulation. After functionalization with the Fc fragment, the changes observed in the bands of amides I, II and III, as well as the N–H stretch at $\sim 3300$ cm$^{-1}$ (highlighted in blue) suggest an increase in the amount of amines in the formulation. Considering that the Fc fragment contains primary amines in its structure, these alterations support the successful conjugation of the targeting ligand to the NPs (Fig. 2c). The link between maleimide and thiol itself is, however, below 500 cm$^{-1}$ in the IR spectra, which is below the spectra range cut-off, and therefore, not shown here. The evaluation of the presence of thiols in the spectrum of the final formulation could also be attempted at around 2550 cm$^{-1}$. However, these bands are weak and easy to overlook (not shown). For these reasons, the extent of the success of this functionalization was further evaluated by elemental analysis, a complimentary technique used to determine the quantity of a particular element within the formulation.

Elemental analysis of the herein developed formulation showed a marked increase in the amount of carbon from the UnTHCPSi NPs to the lignin-encapsulated NPs, as expected, due to the addition of the biopolymer to the nanosystem (Table 1). Also importantly, nitrogen appeared in the formulation only upon functionalization with the Fc fragment, which contains primary amines, supporting the ATR–FTIR data and, consequently, the successful conjugation of the targeting ligand to the NPs (Table 1). Based on the chemical structure of the Fc

**Table 1**
Elemental analysis determination of the mass percentage of nitrogen, carbon and sulfur elements in the NP formulation at different steps of preparation.

| Sample | N, % | C, % | S, % |
|---|---|---|---|
| UnTHCPSi | $N_u$ | $13.11 \pm 3.97$ | $S_u$ |
| UnTHCPSi@LNPs | $N_u$ | $41.39 \pm 2.03$ | $1.05 \pm 0.05$ |
| UnTHCPSi@LNPs-Fc | $1.05 \pm 0.06$ | $41.76 \pm 0.62$ | $1.11 \pm 0.03$ |

$N_u$ = N amount below the detection limit; $S_u$ = S amount below the detection limit. Results are expressed as mean $\pm$ *s.d.* of three independent batches ($n = 3$).

region of IgG, there are *ca.* $0.052 \pm 0.004$ mg of Fc per 1 mg of UnTHCPSi@LNPs.

The morphological properties of the NPs were assessed by TEM. Fig. 3a shows an irregular surface of UnTHCPSi NPs, which becomes smooth after encapsulation with a thin layer of lignin. The functionalization of the NPs with the Fc fragment does not induce visible morphological alterations, as expected (Fig. 3a, upper panel). Additionally, UnTHCPSi NPs do not suffer detectable alterations after being loaded with insulin (Fig. 3a, lower panel). The entrapment into the lignin matrices was equally successful, with the final formulation showing the desired size and shape (Fig. 3a, lower panel). Further TEM images with a higher number of particles per image can be found in Figure S1. The EDX elemental composition analysis showed the presence of the Si peak in UnTHCPSi NPs (Fig. 3b, Spectra 1 and 2, blue arrow), whereas no Si was detected in the surroundings of the NPs (Fig. 3b, Spectrum 3). Results also confirmed the presence of UnTHCPSi NPs inside the lignin matrices due to the appearance of the Si peak in the spectra of both UnTHCPSi@LNPs and UnTHCPSi@LNPs-Fc (Fig. 3b, Spectra 1 and 2, blue arrow), with Si being similarly undetectable in surroundings of the NPs (Fig. 3b, Spectrum 3). Overall, these results confirm the successful development of insulin-loaded, lignin-nano-encapsulated, FcRn-targeted PSi NPs.

### 3.3. pH-Responsiveness of LNPs

Although lignin is an abundant biomaterial, renewable and eco-friendly [21], it has only very recently been considered for drug delivery applications and, particularly, for oral administration [31]. Lignins are, in fact, the main organic polymers present in dietary insoluble fiber, known to resist the digestive process in the GIT [31]. In line with this, it has been suggested that the incomplete ionization of the –COOH groups at acidic pH is not enough to disintegrate lignin molecules, limiting their solubility in such conditions [44]. Hence, the fact that lignin is biocompatible, together with its capacity to remain intact in the harsh stomach conditions triggered the ongoing explorative research around lignin for oral drug delivery applications. Moreover, the dissolution/stability of carboxylated lignin polymers with different carboxylation degrees have been recently investigated, where the lignin used herein was reported to dissolve immediately after incubation at physiological pH [45]. Therefore, we hypothesized that lignin would protect the insulin-loaded UnTHCPSi NPs throughout the GIT, and remain intact while in contact with the intestinal cells. After FcRn-mediated transcytosis, the NPs would reach the blood circulation, and lignin would dissolve, finally releasing insulin.

Hence, the pH-responsive dissolution behavior of the lignin-encapsulated NPs developed in this study was evaluated by incubating the NPs with buffers at different pH values (1.2, 5.5, 6.0, 6.5 and 7.4) from 2 to 30 min. These pH conditions are physiologically relevant for any drug carrier aimed at oral administration, as they mimic the pH variations found from oral intake, throughout the GIT and, ultimately, the blood circulation (after being transported across the intestinal cells) [46]. DLS and TEM were used to evaluate the morphological changes of the NPs throughout the experiment. In the DLS plots (Fig. 4a), the grey dashed lines mark the properties of the NPs (size and PdI, respectively) immediately after preparation, as originally presented in Fig. 2, before
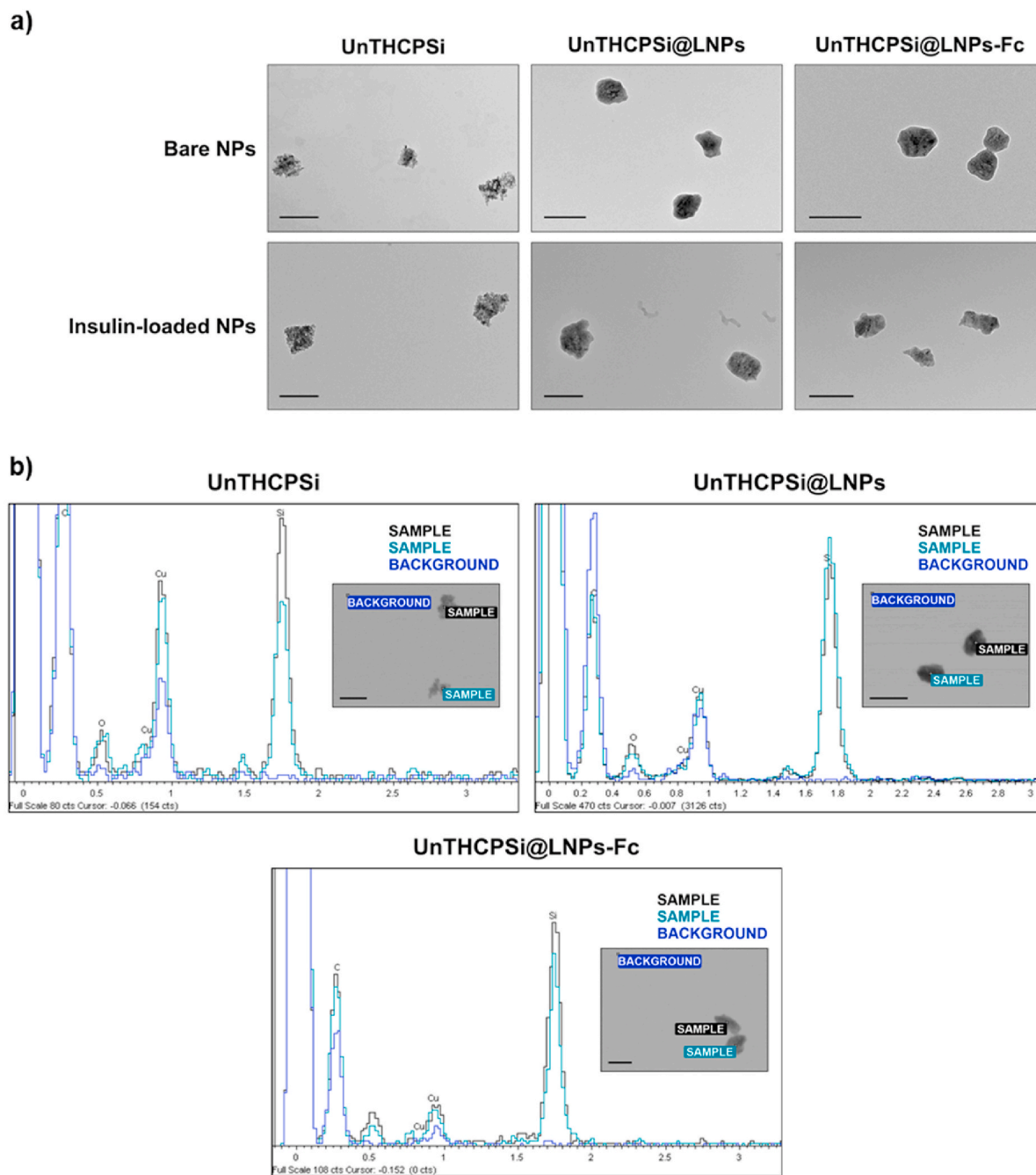
**Fig. 3. Morphological characterization of the NPs. a)** TEM images of bare and insulin-loaded NPs at different steps of preparation (scale bars represent 200 nm); **b)** EDX analysis of the elemental composition of the NPs; spectra 1 and 2 represent the analysis of two different particles, whereas spectrum 3 represents the analysis of the background (scale bars represent 200 nm).

incubation with any of the solvents, and were included to help understanding how much these values are deviating or not from the properties of the original NPs. The DLS data indicated that the lignin matrix remained intact throughout the acidic buffers that mimic the stomach conditions, as well as the upper intestine, where the cellular absorption must occur (Fig. 4a). This is essential to protect insulin from premature release and degradation. Even though the DLS data did not detect any alteration in the size of both UnTHCPSi@LNPs and UnTHCPSi@LNPs-Fc throughout the test, the insulin-loaded UnTHCPSi@LNPs-Fc showed a particularly marked decrease on the size of the NPs when incubated at pH 7.4, which occurred immediately 2 min after incubation (Fig. 4a). This effect may have been triggered by the fact that the initial sizes of insulin-loaded NP were already slightly higher than those of its

unloaded counterpart, as shown in Fig. 2a, resulting in a more noticeable decrease in the particle size upon dissolution of lignin. These results suggest both that lignin can protect insulin from degradation until it reaches the pH conditions of the blood circulation and also that the dissolution process of lignin occurs rapidly. The NPs showed narrow size distribution for all pH conditions and time points tested (Fig. 4a).

The TEM images further elucidated these findings (Fig. 4a), by showing that all NP systems remain intact and with a smooth surface in pH conditions of 1.2–6.5. The subsequent emergence of the irregular surface of the core UnTHCPSi NPs showed that lignin dissolution occurred in a progressive manner, which starts immediately after 2 min of incubation at pH 7.4. These images also showed that the lignin matrices were absent from the formulation after 30 min of incubation at
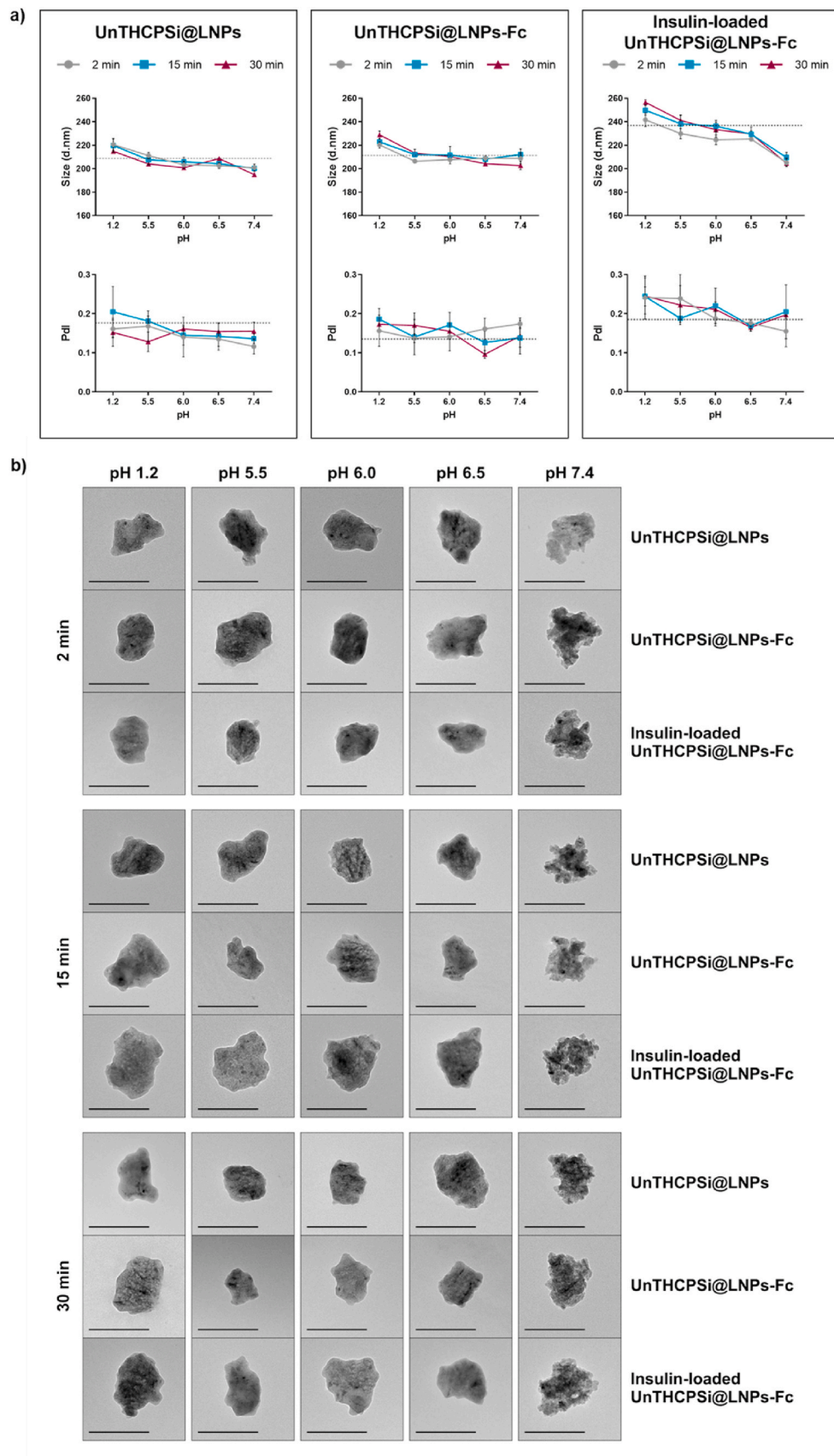
**Fig. 4. pH-Responsive behavior of the NPs.** UnTHCPSi@LNPs, UnTHCPSi@LNPs-Fc and insulin-loaded UnTHCPSi@LNPs-Fc after incubation in different buffer solutions (pH 1.2, 5.5, 6.0, 6.5 and 7.4) for 2, 15 and 30 min. **a)** Size and PdI; results are expressed as mean $\pm$ *s.d.* of three independent measurements of the same batch ($n \geq 3$); **b)** TEM images of the NPs (scale bars represent 200 nm).

pH conditions mimicking the blood circulation. The fact that the DLS did not show any changes in the sizes of bare UnTHCPSi@LNPs and UnTHCPSi@LNPs-Fc may be attributed both to the fact that lignin forms a very thin layer around the core NPs and also to the use of several buffers and different pH conditions, which possibly interfere with the measurements of their hydrodynamic diameters [47]. The TEM images, however, showed that the dissolution of the lignin matrix occurs as initially aimed for this nanosystem. Altogether, these data showed that the NPs remain intact in the pH conditions found throughout GIT, which would enable their interaction with the FcRn-expressing epithelial cells. After transcytosis in their intact form, the NPs should be able to reach

the blood circulation, where the core, insulin-loaded NPs would become exposed, as demonstrated herein.

### 3.4. Drug loading and in vitro drug release studies

As a result of the hydrophobic nature of their core, the lignin NPs fabricated in this study would not suitably serve as insulin carrier alone [36]. Attempting to load insulin in these NPs would result in a very low loading degree and possible leakage during storage. Therefore, the presence of UnTHCPSi as core NPs was needed to ensure proper drug loading. Hence, insulin was loaded into the UnTHCPSi NPs, according to
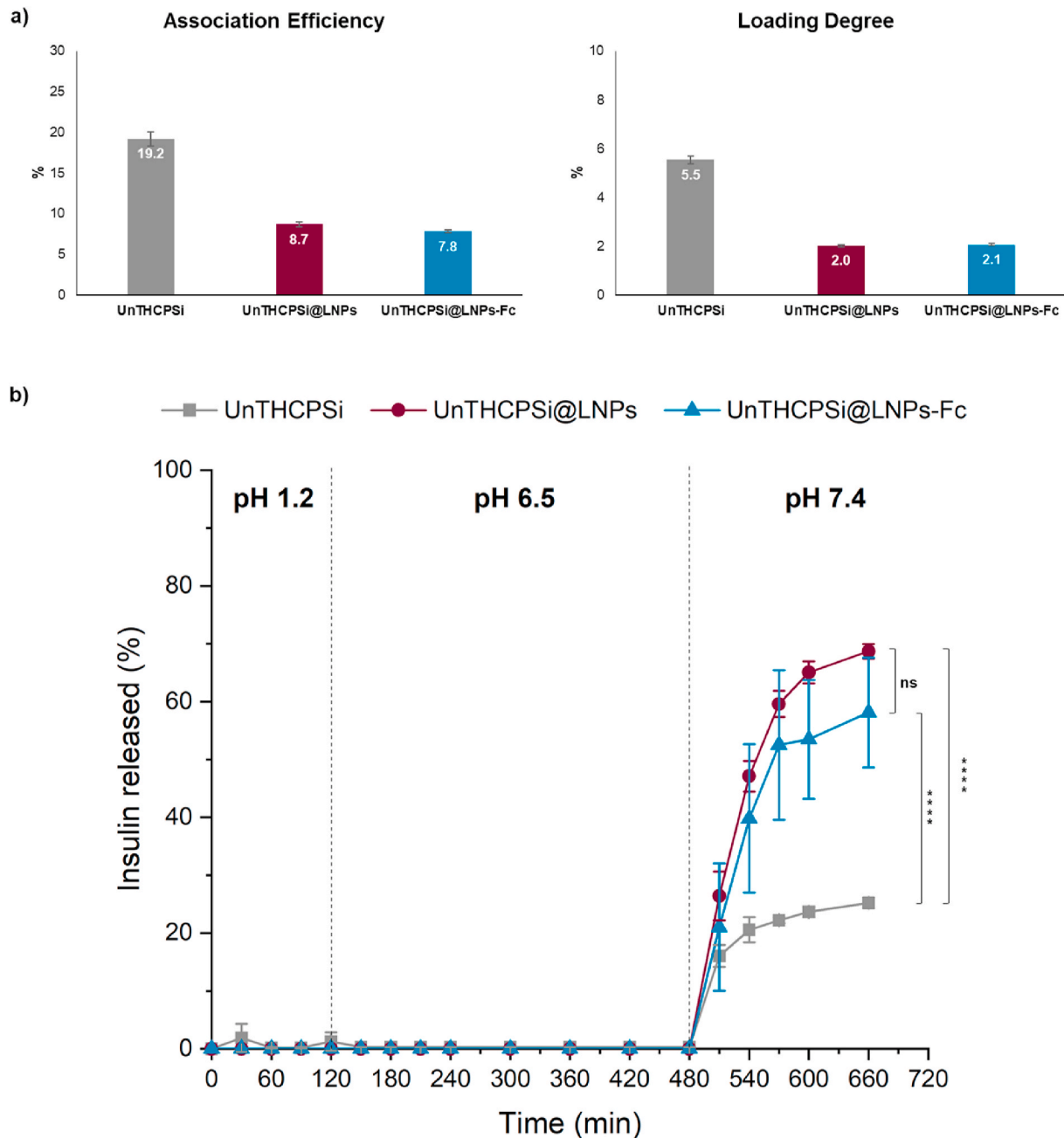


**Fig. 5. AE, LD and *in vitro* insulin release profile of the developed NPs. a)** AE (*w/w*) and LD (*w/w*) of UnTHCPSi, UnTHCPSi@LNPs and UnTHCPSi@LNPs-Fc; **b)** Insulin release profile from the NPs at different steps of preparation; the percentages of insulin released were compared at time points from 15 min to 11 h. The experiments were conducted at 37 °C, under magnetic stirring, with the particles dispersed in different buffer solutions at pH 1.2, pH 6.5 and pH 7.4. Results are expressed as mean ± *s.d.* of three independent batches (*n* = 3). Two-way ANOVA was used for the statistical analyses of the measured values, followed by the Bonferroni *post hoc* test. Data sets were compared at the last time point to the control (UnTHCPSi NPs). The level of significant differences was set at probabilities of *p* < 0.05, **p* < 0.01, ***p* < 0.001, and ****p* < 0.0001. Results are expressed as mean ± *s.d.* of three independent samples (*n* = 3).

a previously optimized immersion method [14,19].

The amount of insulin associated to the NPs was determined by the calculation of the AE and LD, *via* direct method. UnTHCPSi NPs showed an AE (w/w) of 19.2 ± 0.9%, whereas the lignin-encapsulated and the Fc-functionalized NPs showed AEs of 8.7 ± 0.3% and 7.8 ± 0.2%, respectively (Fig. 5a). The decrease observed from the non-encapsulated (UnTHCPSi NPs) to the lignin-encapsulated NPs (both UnTHCPSi@LNPs and UnTHCPSi@LNPs-Fc) is attributed to the loss of insulin during the encapsulation step. However, once the lignin matrix is formed, there is only a minimal difference in the AE of the NPs functionalized with the Fc. The LD (w/w) showed a similar trend, with values of 5.5 ± 0.2% for UnTHCPSi NPs, 2.0% for UnTHCPSi@LNPs and 2.1% for UnTHCPSi@LNPs-Fc. The decrease from the non-encapsulated to the lignin-encapsulated NPs is equally attributed to the fact that UnTHCPSi@LNPs and UnTHCPSi@LNPs-Fc are submitted to more steps of preparation, with eventual loss of insulin, as well as to the increase in their mass, resulting from the addition of lignin, with the mass being accounted for the calculations of the LD.

The *in vitro* release profile of insulin from the NPs was investigated by successively incubating them with buffers at pH 1.2, 6.5 and 7.4, thereby mimicking the passage of the NPs through the different pH conditions found from oral intake to the blood circulation. The duration of the incubation times in the first two buffers (2 and 6 h, respectively) was determined according to the estimated residence time of the NPs in the stomach and intestine [46], whereas the 3 h incubation time at pH 7.4 was chosen based on the achievement of a release plateau during the optimization of the protocol (not shown).

The *in vitro* insulin release profile from UnTHCPSi NPs, UnTHCPSi@LNPs and UnTHCPSi@LNPs-Fc is shown in Fig. 5b. Results showed that lignin protected insulin from being prematurely released at pH 1.2 and 6.5 in both functionalized and non-functionalized NPs. This effect is essential to ensure that the integrity of the NPs is maintained all the way through the GIT, as well as to enable them to reach and interact with the intestinal cells for transcytosis [48]. The drug started being gradually released only when the NPs were incubated at pH 7.4, reaching release values of *ca.* 60–70%. The fact that not all insulin loaded into the NPs was released during this experiment can be ascribed to the interactions between the hydrophobic parts of insulin and the surface of the porous silicon, which limit the release of the protein that becomes irreversibly attached, as previously reported [16]. Surprisingly, UnTHCPSi NPs alone, without being encapsulated into lignin matrices, showed an impaired release of the drug throughout the experiment. Moreover, only minimal amounts were released at pH 1.2, as one would expect, but which may be caused by the abovementioned hydrophobic interactions occurring when dispersed directly in the acidic buffers. These NPs only reached release values of *ca.* 25%. Despite their release profile, in a living organism, the prolonged exposure of the drug in the open pores of the UnTHCPSi NPs to the high enzymatic activity of the stomach would compromise the structure, and therefore, the therapeutic effect of insulin. For these reasons, the lignin matrices are shown to play a crucial role in protecting the drug, while ensuring its adequate release in the target site only. This experiment also supports the translatability of this system to other therapeutic purposes, since UnTHCPSi NPs are a versatile drug carrier, which can be loaded with a variety of drug molecules, with different sizes, molecular structures and properties [40,41].

### 3.5. Characterization of the FcRn expression

Established *in vitro* models grown in specific conditions provide indispensable tools for predicting the behavior of drug delivery systems when in contact with the intestinal microenvironment, and thus, the transport of drugs and/or NPs across the intestinal epithelium. Caco-2/HT29-MTX co-cultures are a widely used *in vitro* system to mimic the physiology of the human intestine [49]. However, the validation of the herein developed targeted NPs depends on the specific expression of the

FcRn by the intestinal cells.

A preliminary test was conducted for validation purposes. Caco-2 and HT29-MTX cells were separately grown on 6-well plates for 7 days. HepG2, a human liver hepatocellular carcinoma cell line, with epithelial morphology, and known for expressing the FcRn [50], were used as positive control. HepG2 were grown in the same conditions. Lysates from Caco-2, HT29-MTX and HepG2 were prepared and analyzed by Western blot. Blots were probed with human FcRn, followed by HRP-conjugated anti-mouse IgG Secondary Antibody. Results showed a 42-kDa band present in both Caco-2 and HepG2 cells, which is consistent with the molecular weight of the FcRn heavy chain (Figure S2). Little or no expression was detected in the HT29-MTX. For these reasons, we carried out the Western blot for characterization of the FcRn expression on Caco-2 cell monocultures and Caco-2/HT29-MTX co-cultures. In this case, cells were grown on Transwell® permeable supports, which provide apical and basolateral compartments, better mimicking the configuration of the human intestine. Lysates were prepared from the Caco-2 cell monocultures and Caco-2/HT29-MTX co-cultures grown for 7, 14 and 21 days, and probed with the primary and secondary antibodies stated above. A Ponceau S staining was used to locate and identify the proteins after electroblotting onto the Western Blot membrane (Figure S3). Western blot results showed that the FcRn expression can be detected in Caco-2 cells immediately after 7 days of culture, as shown by the presence of the 42-kDa band (Fig. 6). This expression showed to increase over the culture period, up to 21 days of culture. A similar trend was observed in the Caco-2/HT29-MTX co-cultures (Fig. 6), with FcRn being detected at every time point tested, confirming the increasing trend over the culture period. α-tubulin was used as loading control (Fig. 6), proving that the differences observed in the FcRn expression were not due to loading inconsistencies nor lack of protein in a lane. Overall, these data support that this model is suitable for *in vitro* evaluation of the behavior of the herein developed FcRn-targeted NPs when in contact with the intestinal microenvironment.

### 3.6. In vitro cytotoxicity studies

Since the NPs developed in this study are expected to interact with the intestinal cells for possible receptor-mediated transcytosis, it is important to evaluate whether any of the materials/compounds used in their preparation induce cellular toxicity. Caco-2 cells, a human colorectal adenocarcinoma cell line, were used to represent the enterocytes, which constitute *ca.* 90% of the intestinal epithelium [49]. HT29-MTX, in turn, constitute the remaining 10%, and were used as mucus-producing cells [49]. When co-cultured, a seeding ratio of 90:10 of Caco-2 and HT29-MTX, respectively, showed to render the best physiological proportions [49].

Here, the cytotoxicity of the developed NPs was investigated on monocultures of Caco-2 and HT29-MTX cells, and on Caco-2/HT29-MTX co-cultures. Cells were exposed to the NPs at different steps of
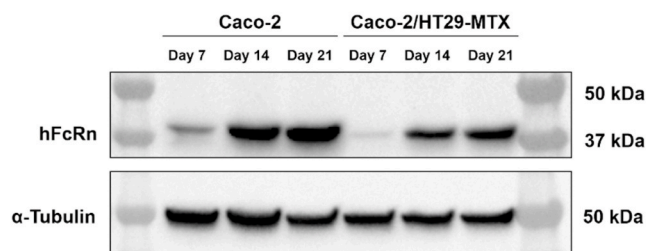


**Fig. 6. Detection of human FcRn by Western blot.** Western blot shows lysates of Caco-2 monocultures and Caco-2/HT29-MTX co-cultures grown for 7, 14 and 21 days, probed with human FcRn, followed by HRP-conjugated anti-mouse IgG Secondary Antibody. anti-α Tubulin was used for loading control.

preparation (UnTHCPSi NPs, UnTHCPSi@LNPs and UnTHCPSi@LNPs-Fc) for 6 and 24 h, with NP concentrations ranging from 25 µg/mL to 400 µg/mL. At these time points, the ATP content in metabolically active cells was measured by the CellTiter-Glo® luminescence assay. The selected cell lines and culture conditions, time points, and NP concentrations are expected to give insights on the NP concentration-dependent toxicity, as well as on the highest concentration that can be used for further studies.

In the Caco-2 monocultures, all NP systems showed mild levels of

toxicity, which occurred in a concentration-dependent manner, with an increase in the toxicity directly proportional to the increase of the NP concentration, both after 6 and 24 h of incubation (Fig. 7). Cell viabilities were, however, always ≥ 84%, even when cells were incubated with the highest NP concentration (400 µg/mL). Results also showed that the different NPs do not induce toxicity when incubated with HT29-MTX cells when using concentrations up to 200 µg/mL (Fig. 7). The highest NP concentration tested, in turn, showed signs of toxicity in this cell line, at both time points tested, presenting a significant difference
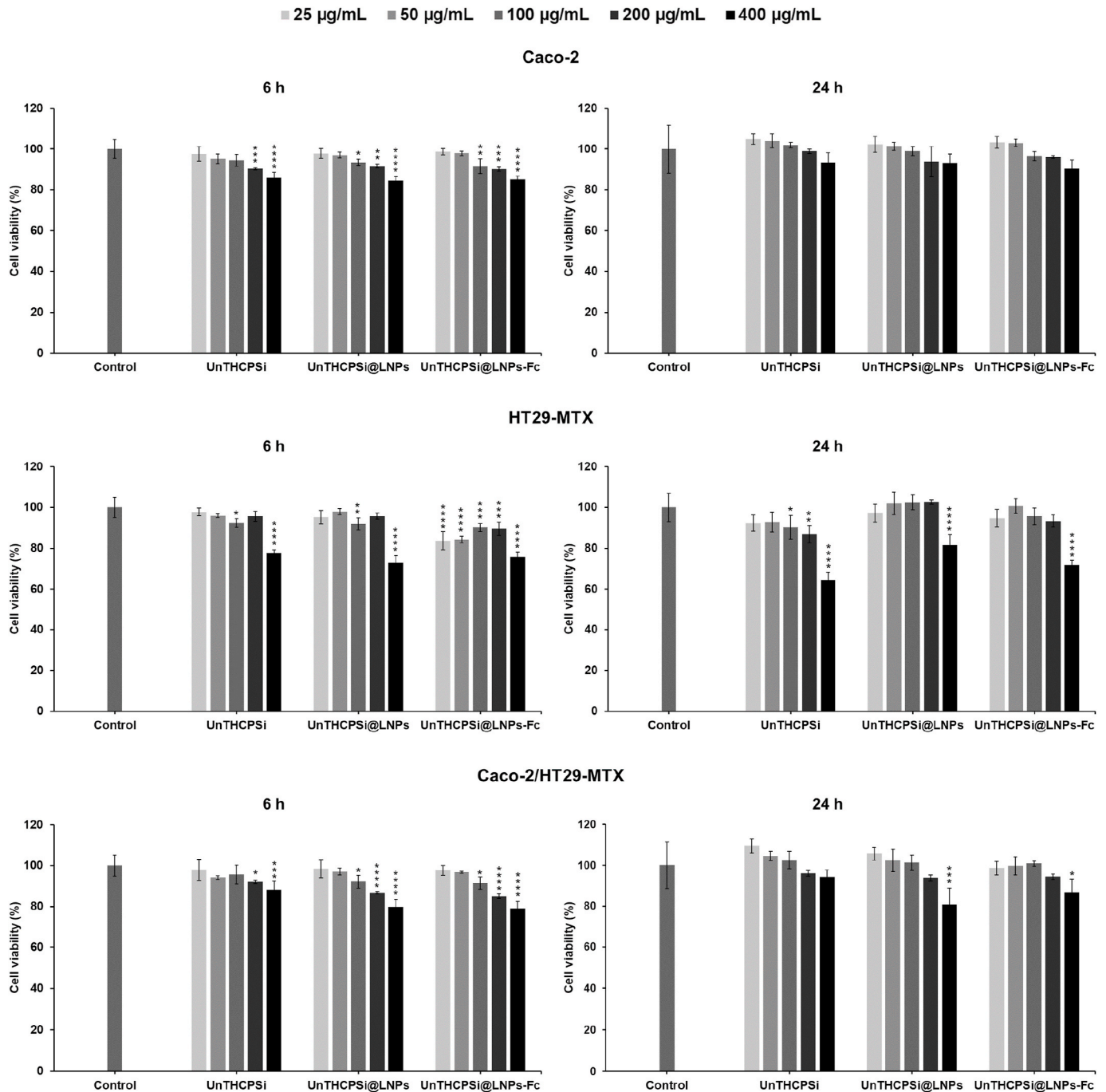


**Fig. 7. Cytocompatibility of the developed NPs.** Cell viability values (%) of Caco-2, HT29-MTX and Caco-2/HT29-MTX (ratio 90:10) when exposed to UnTHCPSi, UnTHCPSi@LNPs, and UnTHCPSi@LNPs-Fc assessed by CellTiter-Glo® luminescence assay. The ATP content was investigated after 6 and 24 h of incubation with the different NPs at different concentrations (25–400 µg). Cells were incubated with cell culture media, as negative control. The incubations were conducted at 37 °C and 5% $CO_2$. Two-way ANOVA was used for the statistical analyses of the measured values, followed by the Bonferroni *post hoc* test. Each data set was compared to the negative control. The level of significant differences was set at probabilities of *$p < 0.05$, **$p < 0.01$, ***$p < 0.001$, and ****$p < 0.0001$. Results are expressed as mean ± *s.d.* of four independent measurements ($n = 4$).

(****$p < 0.0001$) when compared to the control. Nonetheless, these cells make only a very small portion of the intestinal epithelium, and therefore, a minimal toxicity effect is expected to be caused by the NPs in future experiments. In line with this, low levels of toxicity and a concentration-dependent trend were again observed when the different NPs were incubated with the Caco-2/HT29-MTX co-cultures for up to 24 h, even with the highest NP concentration (Fig. 7). The overall cell viabilities were maintained ≥ 79%. Altogether, these results suggest that the final formulation and the materials it contains are biocompatible with the intestinal cells for incubation periods of up to 24 h, and concentrations of up to 400 μg/mL.

### 3.7. Cell–NP interaction studies

Lignin is an optimal candidate for the development of advanced drug delivery systems due to the presence of functional groups on its native surface, as well as the possibility to be chemically modified with the desired functional groups, which then enable the chemical conjugation of targeting ligands [31]. Yet, the transport of the developed NPs via FcRn-mediated transcytosis depends on the success of the interactions between the NPs and the intestinal cells. In this study, the binding ability of the Fc fragments used to functionalize the NPs and, most importantly, the cell–NP interactions were investigated by SPR. SPR is an optical method that allows the sensitive and label-free monitoring of molecular interactions, based on the propagation of waves of surface plasmons on a metal surface upon excitation with p-polarized visible light [51,52].

Firstly, the binding ability of the free Fc fragments was studied through the analysis of their affinity towards protein A. Protein A is expressed on the surface of Gram-positive bacterium *Staphylococcus aureus*, composed of several domains that can bind the Fc portion of IgGs [53]. The strength of this interaction depends on the type of IgG [32]. SPR studies using Protein A immobilized on the surface of gold sensors have shown a great potential for the study of antibody–receptor interactions [54]. Figure S4 shows the SPR PAP responses against time when injecting Fc fragments at concentrations varying from 0.1 to 100 μg/mL in HBSS–HEPES (pH 7.4) on a protein A-covered SPR sensor. With the exception of the lowest concentration tested, all Fc fragment concentrations caused immediate responses in PAP. Also importantly, this process occurred in a concentration-dependent manner, with an increasing PAP upon the gradual increase of the Fc fragment concentration. The highest concentration tested (100 μg/mL) reached a maximum shift of ~550 millidegrees (Figure S4). For the majority of the concentrations, the SPR response reaches a plateau, indicating that the system is at equilibrium, and therefore, that the association and dissociation rates are equal. The equilibrium affinity ($K_D$) of the Fc fragment towards protein A was ~30 μM, which indicates a fairly strong interaction between the two molecules.

While the Fc portion of IgG is expected to bind optimally to protein A at pH 8.2, the highest affinity between the Fc and the FcRn-expressing intestinal cells is reported to occur at pH 6.5 [25]. For this reason, 10 μg/mL samples of Fc in HBSS–HEPES at pH 6.5, 7.4 and 8.2 were injected on gold-coated SPR sensors immobilized with protein A. Interestingly, all samples caused PAP responses immediately after injection, and showed high binding ability towards protein A (Figure S5). Moreover, the binding equilibrium was reached for every sample, and no significant differences on the intensity of binding ability were observed between the different pH conditions. Altogether, these data support the biological activity and functionality of the Fc fragment used in this study and its potential as a targeting ligand for NP surface functionalization.

Lastly, the binding ability of FcRn-targeted NPs to FcRn-expressing intestinal epithelial cells was investigated. Non-targeted NPs (UnTHCPSi@LNPs) were used as control. Prolonged culturing of Caco-2 cells up to 21 days over gold-coated SPR sensors resulted in detachment of the monolayer from the substrate and a reduced cellular survival rate (data not shown). Nonetheless, Caco-2 cells showed to be confluent over

the sensors at day 14 of culture. Also, the Western blot data presented in this study showed that Caco-2 cells already express high levels of FcRn at this stage. Therefore, this experiment was conducted in Caco-2 cells immobilized on gold-coated SPR sensors for 14 days. For this study, the system was primed with HBSS–HEPES–Pen-Strep (pH 6.5) until a stable baseline was achieved. Upon injection with the NPs (100 μg/mL), both targeted and non-targeted NPs caused immediate responses in PAP (Fig. 8). Whereas the results show the occurrence of non-specific interactions between non-targeted NPs and Caco-2 cells, the FcRn-targeted UnTHCPSi@LNPs-Fc presented higher binding ability towards the FcRn-expressing cells throughout the entire experiment (Fig. 8). No signal decrease was observed even after sample injections were stopped and or when the system was being flushed with running buffer, further supporting the strength of these interactions. At the end of the experiment, the binding ability of the FcRn-targeted NPs presented a significant difference (*$p < 0.05$) when compared to the non-targeted NPs. In summary, these data show a noticeable difference between UnTHCPSi@LNPs and UnTHCPSi@LNPs-Fc, and the higher binding ability observed specifically for Fc-functionalized NPs reinforces the potential of FcRn transcytosis as a functional pathway for increasing the intestinal permeation of drug-loaded NPs.

### 3.8. Insulin permeability studies on an in vitro cell culture model

To reach the blood circulation and find the optimal pH conditions to release insulin, the lignin-encapsulated NPs developed in this study need to migrate from the apical to the basolateral side of the intestinal epithelium. Hence, after the Western blot validation of the FcRn expression on the *in vitro* cell culture model, and the promising SPR cellular interaction studies, insulin permeation was investigated across Caco-2/HT29-MTX co-cultures.

The establishment of a confluent monolayer and development of tight junctions was assessed by monitoring the TEER over the culture period. Results showed increasing TEER values until day 9 of culture, then starting to stabilize and even slightly decreasing as the cell differentiation is occurring (Figure S6). Nonetheless, the TEER value of $794 \pm 52\ \Omega\ cm^2$ obtained at the end of the culture period (21 days) supports the successful development of continuous tight junctions [55] and, more
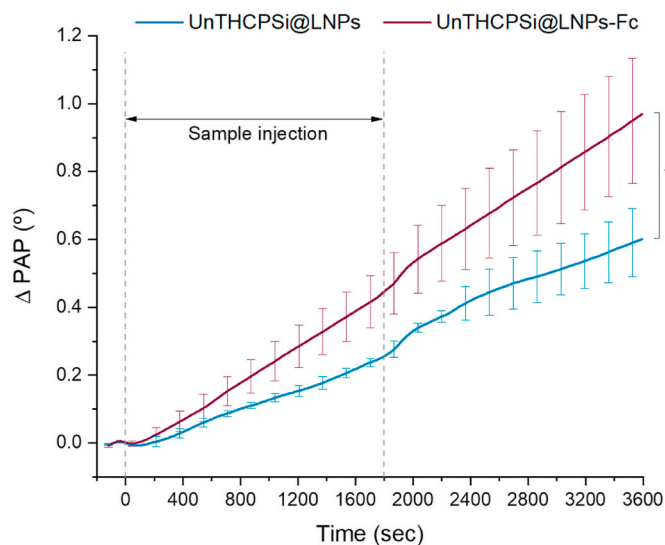


Fig. 8. **SPR analysis of the interaction between FcRn-targeted and non-targeted NPs with Caco-2 cells.** Representative SPR PAP responses to UnTHCPSi@LNPs and UnTHCPSi@LNPs-Fc (100 μg/mL) with Caco-2 cells. Results are expressed as mean ± *s.d.* of three independent injections ($n = 3$). One-way ANOVA was used for the statistical analyses of the values measured at the last time point, followed by the Bonferroni *post hoc* test. The level of significant differences was set at probabilities of *$p < 0.05$.

importantly, the integrity of the cell monolayer in a close resemblance of the *in vivo* scenario.

Results from the insulin cumulative permeability profiles depict an increase in the amount of insulin permeating the intestinal cells immediately after 15 min of incubation, which gradually increases throughout the experiment (Fig. 9a). The permeation rate of insulin from the FcRn-tartgeted UnTHCPSi@LNPs-Fc was faster than the non-targeted NPs and UnTHCPSi NPs alone, presenting, at the end of the incubation period, a statistically significant difference (****$p < 0.0001$) (Fig. 9a). The use of UnTHCPSi NPs as drug carriers may have promoted the levels of insulin permeation observed for the non-targeted systems, which is also in agreement with the non-specific interactions observed in the SPR studies.

The apparent permeability coefficients ($P_{app}$) of insulin were calculated from the permeation profiles across the Caco-2/HT29 monolayers (Fig. 9b). The $P_{app}$ for insulin loaded into UnTHCPSi@LNPs-Fc was always higher than that of UnTHCPSi@LNPs and UnTHCPSi NPs. At the end of the experiment, the $P_{app}$ of UnTHCPSi@LNPs-Fc were *ca.* $2.37 \times 10^{-6}$ cm/s, whereas the $P_{app}$ of UnTHCPSi@LNPs and UnTHCPSi NPs were *ca.* $1.66 \times 10^{-6}$ cm/s and *ca.* $1.01 \times 10^{-6}$ cm/s, respectively. Hence, the insulin that permeated the cell monolayers when loaded into the FcRn-targeted NPs was significantly higher than that loaded into UnTHCPSi@LNPs (**$p < 0.01$) and UnTHCPSi NPs (****$p < 0.0001$) (Fig. 9b). Overall, the addition of the Fc fragment of IgG as a targeting ligand on the surface of the NPs revealed to further increase the insulin permeation across the Caco-2/HT29-MTX co-cultures.

The HPLC data were greatly supported by the microscopic analysis of the behavior of the NPs when in the physiological environment, *i.e.*, the Caco-2/HT29-MTX co-cultures. For this purpose, at the end of the experiment, the excess, non-interacting NPs were washed, and the Transwell® membranes were dehydrated and embedded in epoxy resin for TEM analysis. Ultra-thin sections of the monolayers incubated with the different NP systems and cut in the perpendicular direction are presented in Fig. 9c. Results show normal morphology of the cells kept
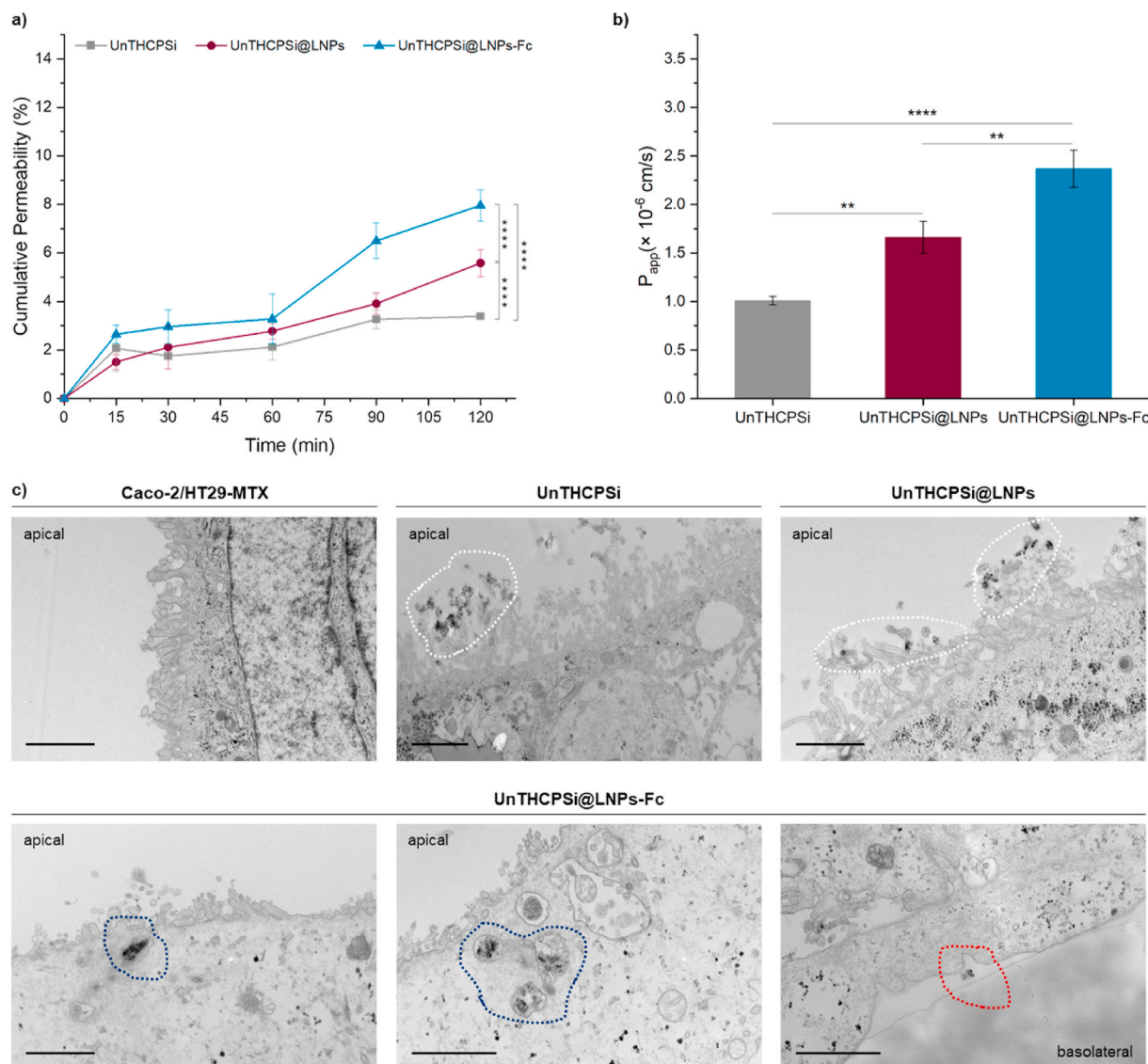


**Fig. 9. *In vitro* permeability studies. a)** Cumulative permeability of insulin across Caco-2/HT29-MTX co-cultures grown in Transwell® permeable supports after incubation with insulin-loaded UnTHCPSi, UnTHCPSi@LNPs, and UnTHCPSi@LNPs-Fc for 120 min. The experiments were conducted in HBSS–HEPES at 37 °C, from the apical (pH 6.5) to the basolateral (pH 7.4) side of the Transwell® supports. **b)** Apparent permeability coefficients ($P_{app} \times 10^{-6}$ cm/s) of insulin across Caco-2/HT29-MTX monolayers calculated from the drug permeation profiles. For **a)** and **b)**, results are presented as mean ± *s.d.* of three different samples ($n = 3$). Two-way ANOVA was used for the statistical analyses of the values measured at the last time point, followed by the Bonferroni *post hoc* test. The level of significant differences was set at probabilities of *$p < 0.05$, **$p < 0.01$, ***$p < 0.001$, and ****$p < 0.0001$. **c)** TEM images of flat embedded ultra-thin Caco-2/HT29-MTX monolayers after 120 min of incubation with buffer, UnTHCPSi, UnTHCPSi@LNPs, and UnTHCPSi@LNPs-Fc for the *in vitro* permeability studies. The scale bars represent 1 μm.

solely with buffer throughout the experiment. Additionally, non-targeted NPs (UnTHCPSi and UnTHCPSi@LNPs) were found in the close vicinities of the cells, amidst the microvilli, but no signs of internalization were detected (Fig. 9c, upper panel, white dashed lines). Also importantly, FcRn-targeted NPs showed not only to be internalized at the apical compartment (Fig. 9c, lower panel, blue dashed lines), but also to be transported across the cells and released in the basolateral compartment (Fig. 9c, lower panel, red dashed lines). These observations are in accordance with the increased insulin permeation detected in the basolateral compartment, thus showing the FcRn-based transcytotic mechanisms and their potential to increase the transport of FcRn-targeted NPs across the tightly organized intestinal epithelium.

Despite the significant progress achieved in the characterization of the developed NPs and on its capacity to increase insulin permeation across *in vitro* cell culture models, *in vivo* studies will be essential to determine the success of this for formulation after being orally administered in a living organism. Since the expression of FcRn in rodents is markedly different than that observed in humans, as it decreases immediately after weaning [56], such studies will require the use of a transgenic mouse model expressing human FcRn (FcRn$^{-/-}$ hFcRn (32) Tg). This model will require the concomitant deletion of the mouse FcRn expression, to avoid discrepancies caused by endogenous expression of the receptor when administering the NPs. More interestingly, any putatively enhanced drug permeation observed in *in vitro* or *in vivo* contexts might be further improved in humans, whose intestinal cells constitutively express FcRn throughout adulthood [56].

## 4. Conclusions

Nanomedicine is revolutionizing the clinical landscape by providing new therapeutic strategies, as well as solutions for the shortcomings of conventional therapies. An ideal nanocarrier system for oral administration in diabetes therapy should circumvent the barriers imposed by the GIT and, ultimately, increase drug permeation across the intestine. Here, we developed and characterized a multistage NP system for the oral administration of insulin. The developed NPs showed to have small size, which revealed to be suitable for intestinal translocation, also showing narrow size distribution. The entrapment of the core insulin-loaded NPs into lignin matrices rendered the nanosystem with pH-responsive properties, ideal for protecting insulin from premature release and degradation in the stomach and upper intestine, but dissolving at the pH conditions that would be found in the blood circulation. The *in vitro* cell culture model used herein showed to express the targeted receptor, FcRn. Moreover, the NPs exhibited low levels of toxicity when incubated with the intestinal cells for periods of up to 24 h. SPR studies revealed that FcRn-targeted NPs display higher binding affinity to Caco-2 cells than their non-targeted counterparts. Insulin permeation across an *in vitro* cell culture model was significantly enhanced when the drug was loaded into NPs functionalized with the Fc fragment of IgG as a targeting ligand to the FcRn. Overall, the porous silicon NPs showed to be a suitable drug carrier, and the lignin-based matrices showed to adequately fit the demands of delivery systems aimed at oral administration. The Fc functionalization showed to play a role in potentiating the success of oral NPs, whose ability to cross the intestinal epithelium is, otherwise, limited. Ultimately, this study provides further possibilities for the development of FcRn-targeted therapies, while fostering the discussion on the reformulation of the administration routes currently in use for diabetes management.

## CRediT authorship contribution statement

**João P. Martins:** Conceptualization, Methodology, Data curation, Writing – original draft, Writing – review & editing. **Patrícia Figueiredo:** Methodology, Review. **Shiqi Wang:** Methodology, Investigation, Review. **Erika Espo:** Investigation. **Elena Celi:** Investigation. **Beatriz Martins:** Investigation. **Marianna Kemell:** Investigation, Review.

**Karina Moslova:** Investigation. **Ermei Mäkilä:** Resources, Review. **Jarno Salonen:** Resources. **Mauri A. Kostiainen:** Resources, Review. **Christian Celia:** Review. **Vincenzo Cerullo:** Resources. **Tapani Viitala:** Methodology, Investigation, Review. **Bruno Sarmento:** Conceptualization, Supervision. **Jouni Hirvonen:** Supervision, Review. **Hélder A. Santos:** Conceptualization, Supervision, Methodology, Resources, Validation, Writing – review & editing.

## Declaration of competing interest

The authors declare no conflict of interest.

## Appendix A. Supplementary data

Supplementary data to this article can be found online at https://doi.org/10.1016/j.bioactmat.2021.08.007.

## References

[1] J.A. Bluestone, K. Herold, G. Eisenbarth, Genetics, pathogenesis and clinical interventions in type 1 diabetes, Nature 464 (7293) (2010) 1293–1300.
[2] J. Reinholz, K. Landfester, V. Mailänder, The challenges of oral drug delivery via nanocarriers, Drug Deliv. 25 (1) (2018) 1694–1705.
[3] T.D. Brown, K.A. Whitehead, S. Mitragotri, Materials for oral delivery of proteins and peptides, Nat. Rev. Mater. 5 (2) (2020) 127–148.
[4] L.S. Rotenstein, B.M. Kozak, J.P. Shivers, M. Yarchoan, J. Close, K.L. Close, The ideal diabetes therapy: what will it look like? How close are we? Clin. Diabetes 30 (2) (2012) 44.
[5] E.P. Herrero, M.J. Alonso, N. Csaba, Polymer-based oral peptide nanomedicines, Ther. Deliv. 3 (5) (2012) 657–668.
[6] N. Dallel, M. Kacem, R.M. Nabouli, M. El May, [Disposal of insulin syringes by diabetic patients. Report of 100 patients], Tunis. Med. 83 (7) (2005) 390–392.
[7] A.C. Anselmo, S. Mitragotri, Nanoparticles in the clinic: an update, Bioeng. Transl. Med. 4 (3) (2019) e10143-e10143.
[8] J.P. Martins, J. das Neves, M. de la Fuente, C. Celia, H. Florindo, N. Günday-Türeli, A. Popat, J.L. Santos, F. Sousa, R. Schmid, J. Wolfram, B. Sarmento, H.A. Santos, The solid progress of nanomedicine, Drug Deliv. Transl. Res. 10 (2020) 726–729.
[9] M.-C. Chen, K. Sonaje, K.-J. Chen, H.-W. Sung, A review of the prospects for polymeric nanoparticle platforms in oral insulin delivery, Biomaterials 32 (36) (2011) 9826–9838.
[10] R.J. Mrsny, Oral drug delivery research in Europe, J. Contr. Release 161 (2) (2012) 247–253.
[11] E.B. Souto, S.B. Souto, J.R. Campos, P. Severino, T.N. Pashirova, L.Y. Zakharova, A. M. Silva, A. Durazzo, M. Lucarini, A.A. Izzo, A. Santini, Nanoparticle delivery systems in the treatment of diabetes complications, Molecules 24 (23) (2019).
[12] H. Ali, B. Weigmann, M.F. Neurath, E.M. Collnot, M. Windbergs, C.M. Lehr, Budesonide loaded nanoparticles with pH-sensitive coating for improved mucosal targeting in mouse models of inflammatory bowel diseases, J. Contr. Release 183 (2014) 167–177.
[13] J.P. Martins, D. Liu, F. Fontana, M.P.A. Ferreira, A. Correia, S. Valentino, M. Kemell, K. Moslova, E. Mäkilä, J. Salonen, J. Hirvonen, B. Sarmento, H. A. Santos, Microfluidic nanoassembly of bioengineered chitosan-modified FcRn-targeted porous silicon nanoparticles @ hypromellose acetate succinate for oral delivery of antidiabetic peptides, ACS Appl. Mat. 10 (51) (2018) 44354–44367.
[14] N. Shrestha, M.-A. Shahbazi, F. Araújo, H. Zhang, E.M. Mäkilä, J. Kauppila, B. Sarmento, J.J. Salonen, J.T. Hirvonen, H.A. Santos, Chitosan-modified porous silicon microparticles for enhanced permeability of insulin across intestinal cell monolayers, Biomaterials 35 (25) (2014) 7172–7179.
[15] J.P. Martins, R. D'Auria, D. Liu, F. Fontana, M.P.A. Ferreira, A. Correia, M. Kemell, K. Moslova, E. Mäkilä, J. Salonen, L. Casettari, J. Hirvonen, B. Sarmento, H. A. Santos, Engineered multifunctional albumin-decorated porous silicon nanoparticles for FcRn translocation of insulin, Small 14 (27) (2018) 1800462.

*J.P. Martins et al.*

[16] N. Shrestha, F. Araújo, M.-A. Shahbazi, E. Mäkilä, M.J. Gomes, B. Herranz-Blanco, R. Lindgren, S. Granroth, E. Kukk, J. Salonen, J. Hirvonen, B. Sarmento, H. A. Santos, Thiolation and cell-penetrating peptide surface functionalization of porous silicon nanoparticles for oral delivery of insulin, Adv. Funct. Mater. 26 (20) (2016) 3405–3416.

[17] L.M. Bimbo, E. Mäkilä, T. Laaksonen, V.-P. Lehto, J. Salonen, J. Hirvonen, H. A. Santos, Drug permeation across intestinal epithelial cells using porous silicon nanoparticles, Biomaterials 32 (10) (2011) 2625–2633.

[18] D.C. Ferreira Soares, S.C. Domingues, D.B. Viana, M.L. Tebaldi, Polymer-hybrid nanoparticles: current advances in biomedical applications, Biomed, Pharma 131 (2020) 110695.

[19] J. Salonen, A.M. Kaukonen, J. Hirvonen, V.P. Lehto, Mesoporous silicon in drug delivery applications, J. Pharmacol. Sci. 97 (2) (2008) 632–653.

[20] R.-j. Dong, D.-f. Zheng, D.-j. Yang, X.-q. Qiu, pH-responsive lignin-based magnetic nanoparticles for recovery of cellulase, Bioresour. Technol. 294 (2019) 122133.

[21] C. Frangville, M. Rutkevičius, A.P. Richter, O.D. Velev, S.D. Stoyanov, V. N. Paunov, Fabrication of environmentally biodegradable lignin nanoparticles, ChemPhysChem 13 (18) (2012) 4235–4243.

[22] P. Figueiredo, K. Lintinen, A. Kiriazis, V. Hynninen, Z. Liu, T. Bauleth-Ramos, A. Rahikkala, A. Correia, T. Kohout, B. Sarmento, J. Yli-Kauhaluoma, J. Hirvonen, O. Ikkala, M.A. Kostiainen, H.A. Santos, In vitro evaluation of biodegradable lignin-based nanoparticles for drug delivery and enhanced antiproliferation effect in cancer cells, Biomaterials 121 (2017) 97–108.

[23] T. Rath, K. Baker, M. Pyzik, R.S. Blumberg, Regulation of immune responses by the neonatal Fc receptor and its therapeutic implications, Front. Immunol. 5 (2014) 664.

[24] E.M. Pridgen, F. Alexis, T.T. Kuo, E. Levy-Nissenbaum, R. Karnik, R.S. Blumberg, R. Langer, O.C. Farokhzad, Transepithelial transport of Fc-targeted nanoparticles by the neonatal fc receptor for oral delivery, Sci. Transl. Med. 5 (213) (2013), 213ra167-213ra167.

[25] J.P. Martins, P.J. Kennedy, H.A. Santos, C. Barrias, B. Sarmento, A comprehensive review of the neonatal Fc receptor and its application in drug delivery, Pharmacol. Ther. 161 (2016) 22–39.

[26] B. Surnar, M.Z. Kamran, A.S. Shah, U. Basu, N. Kolishetti, S. Deo, D.T. Jayaweera, S. Daunert, S. Dhar, Orally administrable therapeutic synthetic nanoparticle for Zika virus, ACS Nano 13 (10) (2019) 11034–11048.

[27] H.A. Santos, J. Riikonen, J. Salonen, E. Mäkilä, T. Heikkila, T. Laaksonen, L. Peltonen, V.P. Lehto, J. Hirvonen, In vitro cytotoxicity of porous silicon microparticles: effect of the particle concentration, surface chemistry and size, Acta Biomater. 6 (7) (2010) 2721–2731.

[28] J.T. Sockolosky, F.C. Szoka, The neonatal Fc receptor, FcRn, as a target for drug delivery and therapy, Adv. Drug Deliv. Rev. 91 (2015) 109–124.

[29] L.M.B. Ferreira, C.P. Kiill, L.N. Pedreiro, A.M. Santos, M.P.D. Gremião, Chapter 5 - Supramolecular design of hydrophobic and hydrophilic polymeric nanoparticles, in: A.M. Grumezescu (Ed.), Design and Development of New Nanocarriers, William Andrew Publishing, 2018, pp. 181–221. https://www.sciencedirect.com/science/article/pii/B9780128136270000053.

[30] G.P. Tandon, K. Pochiraju, 7.8 environmental durability of polymer matrix composites, in: P.W.R. Beaumont, C.H. Zweben (Eds.), Comprehensive Composite Materials II, Elsevier, Oxford, 2018, pp. 131–158.

[31] M.S. Alqahtani, A. Alqahtani, A. Al-Thabit, M. Roni, R. Syed, Novel lignin nanoparticles for oral drug delivery, J. Mater. Chem. B 7 (28) (2019) 4461–4473.

[32] L. Jendeberg, P. Nilsson, A. Larsson, P. Denker, M. Uhlén, B. Nilsson, P.A. Nygren, Engineering of Fc(1) and Fc(3) from human immunoglobulin G to analyse subclass specificity for staphylococcal protein A, J. Immunol. Methods 201 (1) (1997) 25–34.

[33] V.K. Thakur, M.K. Thakur, Recent advances in green hydrogels from lignin: a review, Int. J. Biol. Macromol. 72 (2015) 834–847.

[34] P.C.A. Bruijnincx, B.M. Weckhuysen, Lignin up for break-down, Nat. Chem. 6 (12) (2014) 1035–1036.

[35] P. Figueiredo, K. Lintinen, J.T. Hirvonen, M.A. Kostiainen, H.A. Santos, Properties and chemical modifications of lignin: towards lignin-based nanomaterials for biomedical applications, Prog. Mater. Sci. 93 (2018) 233–269.

[36] P. Figueiredo, C. Ferro, M. Kemell, Z. Liu, A. Kiriazis, K. Lintinen, H.F. Florindo, J. Yli-Kauhaluoma, J. Hirvonen, M.A. Kostiainen, H.A. Santos, Functionalization of carboxylated lignin nanoparticles for targeted and pH-responsive delivery of anticancer drugs, Nanomedicine 12 (21) (2017) 2581–2596.

[37] Q. Yang, X. Pan, Correlation between lignin physicochemical properties and inhibition to enzymatic hydrolysis of cellulose, Biotechnol. Bioeng. 113 (6) (2016) 1213–1224.

[38] G.T. Hermanson, Chapter 4 - zero-length crosslinkers, in: G.T. Hermanson (Ed.), Bioconjugate Techniques, third ed., Academic Press, Boston, 2013, pp. 259–273.

[39] B. Ahvazi, É. Cloutier, O. Wojciechowicz, T.-D. Ngo, Lignin profiling: a guide for selecting appropriate lignins as precursors in biomaterials development, ACS Sustain. Chem. Eng. 4 (10) (2016) 5090–5105.

[40] L.M. Bimbo, M. Sarparanta, H.A. Santos, A.J. Airaksinen, E. Mäkilä, T. Laaksonen, L. Peltonen, V.-P. Lehto, J. Hirvonen, J. Salonen, Biocompatibility of thermally hydrocarbonized porous silicon nanoparticles and their biodistribution in rats, ACS Nano 4 (6) (2010) 3023–3032.

[41] V. Stojanovic, F. Cunin, J.O. Durand, M. Garcia, M. Gary-Bobo, Potential of porous silicon nanoparticles as an emerging platform for cancer theranostics, J. Mater. Chem. B 4 (44) (2016) 7050–7059.

[42] S.A. Kulkarni, S.-S. Feng, Effects of particle size and surface modification on cellular uptake and biodistribution of polymeric nanoparticles for drug delivery, Pharm. Res. (N. Y.) 30 (10) (2013) 2512–2522.

[43] P. Foroozandeh, A.A. Aziz, Insight into cellular uptake and intracellular trafficking of nanoparticles, Nanoscale Res. Lett. 13 (1) (2018), 339-339.

[44] M.H. Sipponen, H. Lange, M. Ago, C. Crestini, Understanding lignin aggregation processes. A case study: budesonide entrapment and stimuli controlled release from lignin nanoparticles, ACS Sustain. Chem. Eng. 6 (7) (2018) 9342–9351.

[45] P. Figueiredo, M.H. Sipponen, K. Lintinen, A. Correia, A. Kiriazis, J. Yli-Kauhaluoma, M. Österberg, A. George, J. Hirvonen, H.A. Santos, Preparation and characterization of dentin phosphophoryn-derived peptide-functionalized lignin nanoparticles for enhanced cellular uptake, Small 15 (24) (2019) 1901427.

[46] F. Araújo, J. das Neves, J.P. Martins, P.L. Granja, H.A. Santos, B. Sarmento, Functionalized materials for multistage platforms in the oral delivery of biopharmaceuticals, Prog. Mater. Sci. 89 (2017) 306–344.

[47] G.E. Borgstahl, How to use dynamic light scattering to improve the likelihood of growing macromolecular crystals, Methods Mol. Biol. 363 (2007) 109–129.

[48] L. Liu, W. Yao, Y. Rao, X. Lu, J. Gao, pH-Responsive carriers for oral drug delivery: challenges and opportunities of current platforms, Drug Deliv. 24 (1) (2017) 569–581.

[49] F. Araújo, B. Sarmento, Towards the characterization of an in vitro triple co-culture intestine cell model for permeability studies, Int. J. Pharm. 458 (1) (2013) 128–134.

[50] L. D'Hooghe, A.D. Chalmers, S. Heywood, P. Whitley, Cell surface dynamics and cellular distribution of endogenous FcRn, PloS One 12 (8) (2017) e0182695-e0182695.

[51] N. Granqvist, H. Liang, T. Laurila, J. Sadowski, M. Yliperttula, T. Viitala, Characterizing ultrathin and thick organic layers by surface plasmon resonance three-wavelength and waveguide mode analysis, Langmuir 29 (27) (2013) 8561–8571.

[52] O.K. Kari, T. Rojalin, S. Salmaso, M. Barattin, H. Jarva, S. Meri, M. Yliperttula, T. Viitala, A. Urtti, Multi-parametric surface plasmon resonance platform for studying liposome-serum interactions and protein corona formation, Drug Deliv. Transl. Res. 7 (2) (2017) 228–240.

[53] A. Forsgren, J. Sjöquist, Protein A" from S. aureus. I. Pseudo-immune reaction with human gamma-globulin, J. Immunol. 97 (6) (1966) 822–827.

[54] T. Champion, A. Beck, Capture of the human IgG1 antibodies by protein A for the kinetic study of h-IgG/FcγR interaction using SPR-based biosensor technology, Methods Mol. Biol. 988 (2013) 331–343.

[55] C. Hilgendorf, H. Spahn-Langguth, C.G. Regårdh, E. Lipka, G.L. Amidon, P. Langguth, Caco-2 versus caco-2/HT29-MTX Co-cultured cell lines: permeabilities via diffusion, inside- and outside-directed carrier-mediated transport, J. Pharmaceut. Sci. 89 (1) (2000) 63–75.

[56] D.C. Roopenian, S. Akilesh, FcRn: the neonatal Fc receptor comes of age, Nat. Rev. Immunol. 7 (9) (2007) 715–725.